CORAL
A Cosmic Ray experiment in and above the LHC tunnel
ADDENDUM

V. Avati, L. Dick[o], K. Eggert[*], A. Zinchenko[a]
CERN, Geneva, Switzerland

C. Taylor
Case Western Reserve University, Cleveland, OH, USA

E. Casimiro Linares, A. Zepeda
Cinvestsav-IPN, Mexico City, Mexico

R. Orava, M. Karhunen, J. Ström[b]
Helsinki Institute of Physics, Helsinki, Finland

S. Akimenko, V. Ronjin, V. Tikhonov, E. Vlassov,
IHEP, Institute for High Energy Physics, Protvino, Russia

V. Berezinsky, F. Vissani
Laboratori Nazionali del Gran Sasso and INFN, Italy

L. Jones
University of Michigan, MI, USA

S.K. Gupta, A. Jain, K.C. Ravindran, S.C. Tonwar and K. Viswanathan
Tata Institute of Fundamental Research, Mumbai, India

Y. Hayashi, S. Kawakami, T. Yoshikoshi
Osaka City University, Osaka, Japan

J. Kangas, J. Peltoniemi, M. Vallinkoski
University of Oulu and Sodankylä Geophysical Observatory, Finland

J. Ridky, P. Travnicek
FzU, Institute of Physics of the C.A.S. High Energy Physics Division,
Prague, Czech Republic

D. Nosek
IPNP, Institute of Particle and Nuclear Physics, Faculty of Mathematics and Physics,
Charles University, Prague, Czech Republic

A. Fernandez, E. Gamez, R. Lopez, S. Roman
Universidad Autonoma de Puebla, FCFM-UAP, Puebla, Mexico

A. Karjalainen, M. Korhonen, A. Mattila, N. Patrikainen, J. Pennanen, M. Rahkala
Rovaniemi Polytechnic, Rovaniemi, Finland

C. Grupen, A. Mailov[c]
University of Siegen , Siegen, Germany

I. Kirov. J. Stamenov, S. Ushev, Hr. Vankov
Institute for Nuclear Research and Nuclear Institute, Sofia, Bulgaria

N. Shivarov, B. Stojanov, R. Zahariev
Central Laboratory of Mechatronics and Instrumentation, Bulgarian Academy of Sciences,
Sofia, Bulgaria

J. Strauss
Institute for High Energy Physics, Vienna, Austria

J. Kempa
Warsaw University of Technology, Warsaw, Poland

A. Akhperjanian, Y. Margaryan, L. Pogossyan, V. Sahakian
Yerevan Physics Institute, Yerevan, Armenia

[o] retired from CERN
[*] Contact person
[a] visitor from Joint Institute for Nuclear Research (JINR), Dubna, Russia
[b] visitor from ARCADA Polytechnic, Helsinki, Finland
[c] on leave from Baku University, Azerbaijian

Contents

1 Questions addressed to the CORAL collaboration

1.1 Introductory Remarks

The following questions were raised, either by the referees, or in the closed-door discussions of the SPSC and reported to us by the referees. Following discussions with them, we have slightly edited the questions, combining questions with a common thrust in order to be able to address them as efficiently as possible.

1.2 Questions addressed to the CORAL collaboration

1. Determination of Primary Particle Composition
   (a) How does CORAL compare with the KASCADE, MACRO and Baksan experiments in terms of statistics, $\ln(A)$ resolution, etc.?
   (b) How does the resolution of $\ln(A)$ vary as a function of the depth of the underground muon array? Is the ALEPH cavern close to optimal?
   (c) What is the resolution of $\ln(A)$, event-by-event, as a function of energy using N_μ vs. N_e?
   (d) What are the systematic errors? How sensitive is the $\ln(A)$ determination to the Monte Carlo? How can the other handles CORAL has on the composition of the primary particles, such as the ability to determine particle composition from the radial distribution of the muons, or the ability to determine the height of an event, be used? Do you have a way to calibrate at low energies with direct measurements?

2. How well can the height of the primary interactions be determined, and what use can be made of this information? Show distributions of the height determinations for p, Fe, or for primary production of multi-muon events as a function of the core position, the energy, etc.

3. What is the significance of the excess of very high multiplicity cosmic ray multimuon events seen in the ALEPH detector?

4. Do you expect that cross sections for novel processes (such as Disoriented Chiral Condensates, Centauros, or QGP) may be large enough to stand out above backgrounds due to ordinary interactions within the shower? How reliable are the tails of the distributions? How well can you identify signs of new physics above the tails? Have any relevant simulations been done (or could they be)?

5. What is the angular resolution of the surface array as a function of energy? Can this be used to help with the height determination?

6. What would you gain if you had
   (a) a larger surface array?
   (b) a larger underground muon array?
   (c) a surface muon array?
   In other words, is the present design close to optimal?

7. Can you present detailed milestones for the project? Who will do what, and when? May we have a tentative money matrix with planning?

8. Can you compare the acceptance of the CORAL detector with the one of a LHC detector like ALICE?

2 General Considerations

2.1 Principal Objectives

– Studies on the energy dependence of relative composition of cosmic ray flux below, around and above the Knee

– Search for signature of exotic phenomenon such as Centauro and anti-Centauro events, Halo events, Disoriented Chiral Condensates, Quark-Gluon Plasma

– Search for signature of new forward-physics through a detailed study on the frequency and structure of muon bundles

2.2 Observational Methods

Of the 4 major observable components of air showers in the lower atmosphere, namely, electrons-photons, Cherenkov photons, hadrons and muons only the last two carry significant imprint of the forward-physics processes that may have occurred in the first few interactions during the development of the cascade shower. Though the development of the electron-photon and Cherenkov photon cascades are influenced strongly by particles produced in the extreme forward region, large fluctuations in the atmospheric levels of the first few interactions and superposition of a large number of interactions occurring lower down in the atmosphere manage to hide the information about the first few interactions.

The observable electron-photon component at the ground level is influenced strongly by the fluctuations in the level of the first few interactions and the elemental nature of the primary particle. For example, the shower size near sea level (altitudes $\leq 2000m$) for a proton-initiated shower with the first interaction at 50 gcm^{-2} level is almost a factor of 2 smaller than for a shower starting at 150 gcm^{-2} level in the atmosphere. Similarly, the observable shower size near sea level is more than a factor of 2 smaller for showers initiated by iron nuclei primaries as compared to proton primaries.

While these facts cause large uncertainty in the determination of primary energy from observations on shower size, they are very helpful in providing additional discriminating power for various studies when combined with observations of muons as proposed for the CORAL experiment. Note that similar discriminatory power is not available for studies based on observations of the hadron component as the electron-photon and hadron component are affected similarly by various physical processes mentioned above.

Observations near sea level on the high energy hadron component also lose their sensitivity to details of forward physics and exotic interactions due to serious experimental limitations on studies of individual high energy hadrons in a background of a large number of lower energy hadrons produced in the lower atmosphere resulting in overlap of cascades in the detector. Early studies by the Tata Institute group using small-area but deep (1.4 m^2, 750 g cm^{-2} Fe) calorimeter and a relatively large visual detector (multiplate cloud chamber with $\sim 2m^2$ area and 280 g cm^{-2} Fe absorber) and recent studies with a very large, finely-segmented and deep calorimeter by the KASCADE collaboration have highlighted these features of the hadron component.

Spatial and temporal characteristics of the Cherenkov photon component of air showers lose their sensitivity to details of the first few interactions, as mentioned above, since most of the observed photons are produced closer to the shower maximum. Temporal studies on Cherenkov photons have been used for measurement of elemental abundances in primary flux but these depend very sensitively on the determination of the position of shower axes and also details of Monte Carlo simulations, particularly, requiring tracking of individual electrons. A combination of studies on Cherenkov radiation with studies on muons offers some advantages but at a very significant loss of observational efficiency due to the requirement of nights without low level

fog, clouds and moon.

Studies on the longitudinal development of air showers in the atmosphere also provide valuable information on the composition of primary flux at extremely high energies ($\geq 10^{17}$ eV but these are not relevant for studies at primary energies near the 'knee' in the energy spectrum.

2.3   Observations on muon component

Early studies on the muon component (alone) focussed on the determination of muon flux and charge ratios using small area detectors at various depths underground corresponding to various energy thresholds. These studies were useful in learning about interactions of muons as well as the energy spectrum of protons and light nuclei at lower energies, up to a few TeV. Attempts were made to learn about production cross-section of short-lived particles (charm) at high energies through detection of flux of 'prompt' muons.

Following the development of GUT theories in the 1970's, very large area detectors were installed at various depths underground searching for events bearing signatures of proton decay. These detectors also served a very useful purpose for studies of the flux of high energy multi-muon events. However, in the absence of any information about the energy of the primary nuclei producing these muon-bundles in the atmosphere, these studies have not yielded any significantly new information on forward-physics and exotic interactions. Detailed studies for determination of the elemental composition of primary cosmic ray flux have been carried out using multiplicity distributions for muons observed deep underground (e.g. MACRO experiment). However, the fact that different regions of multiplicity distributions are contributed by primary particles of very different energies and different nuclear groups, poses a severe problem for synthesizing a reliable model of the energy dependence of various nuclear groups in primary flux at $\sim PeV$ energies. In addition, there seem to be some internal consistency problems with interpretation of all observations by a single experiment as well as observations by different experiments.

2.4   Simultaneous observations on electron-photon and muon component in air showers

It has been long realised that the highest sensitivity for observations on forward physics, exotic particle interactions and nuclear composition of primary flux can be achieved by simultaneous observations on the electron-photon and muon components. Very simple arguments can be made to justify this view:

A primary proton of energy E, after travelling one interaction mean free path in the atmosphere produces, on the average, secondary multiplicity of about $K E^{0.25}$, where K is a constant.

On the other hand, a primary nucleus of same total energy but with A nucleons, in a simple superposition model, produces $A \times K (E/A)^{0.25}$ secondaries at a similar depth in the atmosphere, that is $A^{0.75}$ larger. The average energy of these secondaries, mostly pions and kaons, is also lower by a similar factor $A^{0.75}$, thereby increasing their decay probability. Detailed simulations show that the number of lower energy ($E^{\mu} \leq 100$ GeV muons near sea level is, on the average, larger by a factor of about 3 in showers initiated by iron nuclei, compared to proton-initiated showers of the same total energy.

Further, the average energy of neutral pions produced in showers initiated by iron nuclei is much lower even though their number is larger. Electron-photon cascades initiated by these lower energy pions develop faster in the upper atmosphere resulting in larger attenuation in the lower atmosphere. Again, detailed simulations show that the average number of electrons in the lower atmosphere (altitudes $\leq 2000m$), in showers initiated by iron nuclei is a factor of about 2-3 smaller than in proton-initiated showers of the same total energy.

3

It is very significant that these two effects, the increase in muon number and decrease in electron number in heavy nuclei-initiated showers are in opposite direction, which helps in magnifying the observable differences between showers initiated by heavy nuclei and lighter nuclei. Therefore, simultaneous observations on the electron-photon and the muon component offer the best discriminating power for studies on the primary composition. However, good measurements on muon component require very large area detectors under thick absorbers (or underground) while good and simultaneous measurements on the electron-photon component require a dense array of unshielded detectors spread over a large area just above the muon detectors, putting some restrictions on the surface topography.

Note that a larger seperation between the shower array on the surface and muon detectors deep underground results in a smaller geometric acceptance factor for studies of electron-muon correlations which may cause severe statistical problems, e.g. EAS-TOP and MACRO and SOUDAN experiments. Though studies on higher energy muons, deeper underground, may be preferred due to their containment within smaller detector areas, most of the observations in the past have suffered from statistical problems as mentioned above.

It is noteworthy that electron-muon correlation studies started as early as 1960's with small area detectors for both electrons and muons, for example, by the Tata Institute group at Kolar Gold Fields and by the Moscow University group with a magnet spectrometer at a shallow depth on the University campus. While many experiments have been carried out over the last 40 years using lower energy ($E_\mu \leq 10 GeV$) muons detectors, there have been only a few experimental studies on high energy muons. Unfortunately, most of these studies have not yielded satisfactory results either due to the smaller area of muon detectors or due to statistical problems associated with smaller geometric acceptance factors. Therefore, it is essential that new studies be carried out with large area detectors at moderate muon energies with large geometric acceptance factors.

Looking at the discriminating power of electron-muon correlations for studies on primary composition, it is clear that good sampling of both components is essential to exploit the expected differences between showers initiated by lighter and heavier nuclei. This can be easily achieved for the electron component by the use of a larger number of unshielded detectors in a dense configuration of the shower array spread over an area of radius ~ 100 m since the lateral distribution of electrons is quite steep. On the other hand, good sampling of the muon component requires much larger area detectors, particularly for lower energy muons due to their relatively flatter lateral distribution, and these detectors should also be spread out over a larger area. These practical difficulties however become less and less serious as one goes for higher and higher energy muons.

The above considerations suggest that muons of moderate energies, $E_\mu \sim 50-200$ GeV seem to offer the best choice for studies on primary composition, particularly at primary energies overlapping the 'knee' in the energy spectrum. It is interesting that a similar conclusion is also reached for studies on 'forward-physics' as well as exotic interactions. This is mainly due to the fact that the average production height of the observed muons increases almost linearly with increasing muon energies. Thus, studies on lower energy muons offer almost no information on 'forward-physics' and exotic interactions due to the fact that most of them are the result of decay of pions produced lower down in the upper atmosphere in a large number of lower energy interactions. This large number of muons produced in 'normal' interactions may thus hide the information on the few 'exotic' interactions that may have occurred in the early part of the development of the hadron cascade.

Studies on very high energy muons produced in the first or the first few interactions may offer the best possibility of observing signals of new processes in particle interactions at the very highest energies. But simple arguments based on decay probability of very high energy

4

pions show that such processes may be unobservable with very high energy muons. This is due to the fact that high energy pions, say, 1.4 TeV, produced in interactions of 1000 TeV protons, at an average height of 20 km (depth corresponding to one interaction length) would most likely interact in the next 100-200 gcm^{-2} (~ 10 km) rather than decay as the mean decay length for these pions is nearly 80 km. Even pions produced in the second generation are more likely to interact than decay. Due to this dominance of interaction over decay for higher energy pions, simulations show that the number of muons in a shower increases with energy only as $E_o^{0.8}$. These considerations lead to the conclusion that studies on moderate energy, $E_\mu \sim 100$ GeV, may offer the best chance of observing some features of 'forward-physics' and 'exotic' interactions such as Centauros, anti-Centauros, DCC, QGP, etc.

Several studies carried out on high energy muons have confirmed the necessity of using finely segmented tracking detectors for measurements on muon multiplicities. This is due to the fact that at depths larger than a few radiation lengths, the muon and associated electron-photon component produced by muons through their electromagnetic interactions in the rock are in equilibrium. Low energy cascades accompanying high energy muons are spread over a few metres due to scattering in the rock above the detector and can cause significant errors in measurement of the frequency of large multiplicity events with detectors having poor spatial resolution.

3 Detailed Response of the CORAL Collaboration

3.1 Determination of Primary Particle Composition

The precise determination of the composition of cosmic ray primaries as a function of the energy is one of the central problems in the understanding of the cosmic ray particle spectrum. It is a great advantage of the CORAL experiment that it has several methods that can be used to discriminate between different types of cosmic ray primaries on an event-by-event basis.

3.1.1 Comparison of CORAL with other experiments

The standard technique, used by almost all experiments with a surface array, consists of a comparison of the electromagnetic shower on the surface with the muon number either on the surface (KASCADE, Casa-Mia) or underground at various depths (CORAL,MACRO,Baksan, etc). For a comparison, some of the experiments are listed in Table 3.1 together with their main characteristics, such as muon momentum threshold, size, resolution and integrated measurement time. In addition to this standard technique, CORAL can also measure the lateral muon distribution and the shower height, both of which also depend on the primary particle. These different methods will help to reduce the systematic errors which presently limit almost all experiments.

3.1.2 CORAL is at an optimal depth

To demonstrate the features of the CORAL experiment we have compared it in a very simplified way with two other experimental scenarios: KASCADE, which is situated at the surface, and MACRO which is deep underground. The CORAL analysis was applied for a muon momentum cut of 3 GeV (close to the surface) and 1 TeV (deep underground). The two-dimensional plots of the muon and electron numbers for proton- and iron- induced showers are given in Figs. 3.1- 3.3 for the two above scenarios, to be compared with the CORAL proposal.

The deep underground scenario is inferior in many ways to the CORAL situation. Because the muon number is reduced by a factor 60, the separation between proton and iron is lacking statistics and hence much worse. For the same reason, the energy determination for an individual event is almost impossible, as is the detailed study of the structure of muon bundles. The distance between the surface and the underground arrays is increased by about a factor five which would require increasing the area of the surface array by a factor of 25 in order to maintain the same angular acceptance.

The shallow scenario looks similar to the CORAL set-up when separation curves are compared. Some aspects, however, are not taken into account in the simulation. For example, the muon density is larger by a factor of three in the center of the shower, which makes the muon tracking more complicated and indeed almost impossible for high-energy showers. Hadron punch-through further complicates the tracking. The detector is swampt by low energy muons because of the lower (3 GeV) muon energy threshold. These come dominantly from hadron decays from interactions late in the shower development. They are therefore more calorimetric in nature and obscure the information from the high energy muons from the first interactions.

We have also studied the separation curves for momenta above 20 and 200 GeV with the result that they are all similar. The optimization is therefore based on geometrical acceptance arguments involving the depth of the underground muon array below the surface air shower array, on the ability to reconstruct high multiplicity muon bundles and determine their structure (including the determination of the effective height of the interaction), and on the sensitivity to exotic interactions and the ability to characterize them via muons. Taking all these considerations into account we believe that the momentum cut of 70 GeV is close to an optimum.

6

Experiment	MSU	Baksan	Frejus	KGF	LVD	MACRO
Energy cut-off, TeV	0.010	0.22 1.3 2.0 3.2	3.2	>3 (<>=7)	~1.3	1.3
Detector area, m^2	36.4	16x16	6x12.3	6x6	13x6.3 (one tower from 5)	12x76.5
Detector type	Geiger counters	liq. scint.	flash chamb.	prop. count.	LST+liq. scint.	streamer tubes
Detector resolution, mm	-	700	5	100	9	30
Measurement time, x10^3 hours*		69	25	48	22	6

Experiment	NUSEX	SOUDAN-2	Homestake	KASCADE	CORAL
Energy cut-off, TeV	3.5	0.7	2.6	0.002	0.07
Detector area, m^2	3.5x3.5	8x14	16x8	122 (distributed over 20x16 m)	200 (distributed over 20x20 m)
Detector type	LST	plastic drift tubes	liq. scint.	MWPC	drift chamb. (16 planes)
Detector resolution, mm	10	6	300	7x14	1
Measurement time, x10^3 hours*	44	6	13	5.4	16 (for 3 years)

*) Approximate values. Some results from some experiments are based on different measurement times.

Table 3.1. Characteristics of experiments for cosmic muon studies
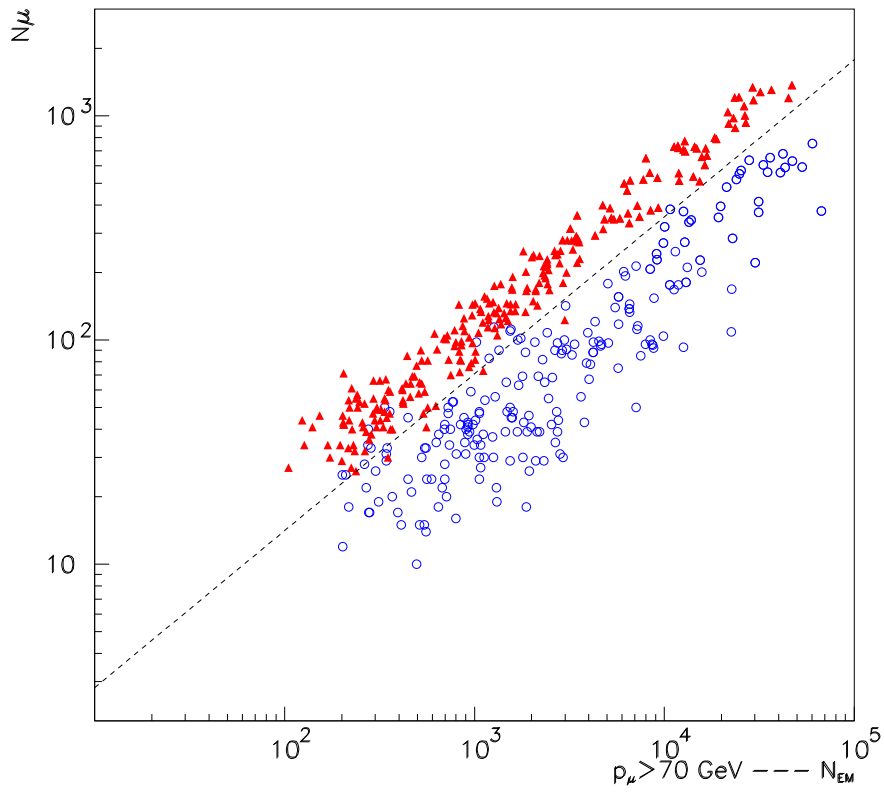
ϑ<15 − 0<R<10

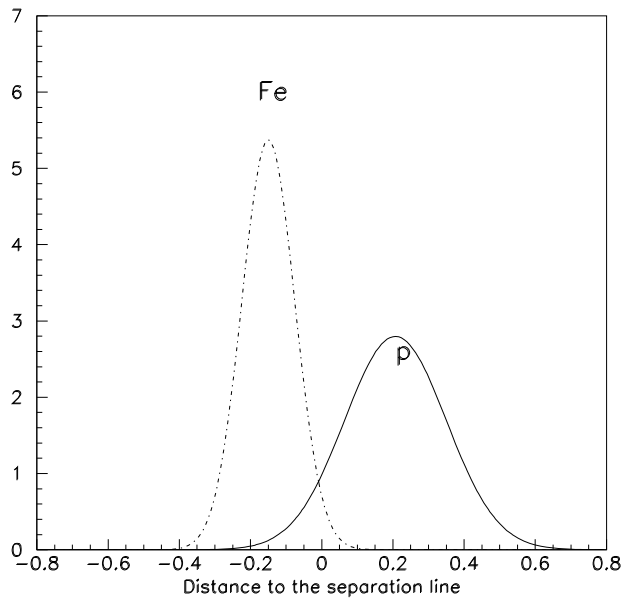*Figure 3.1. CORAL scenario with $p_\mu >70$ GeV/c. Muon number vs electron number for almost vertical showers (zenith angle $\theta < 15^o$) hitting the muon array with a shower core distance to the array center of less than 10 m. Triangles are Fe- and circles p-induced showers. The projection vertical to the separation line is also given.*
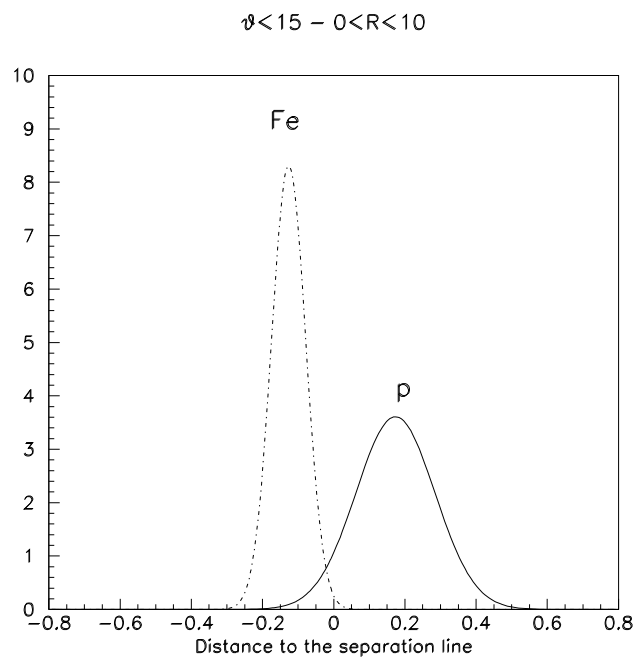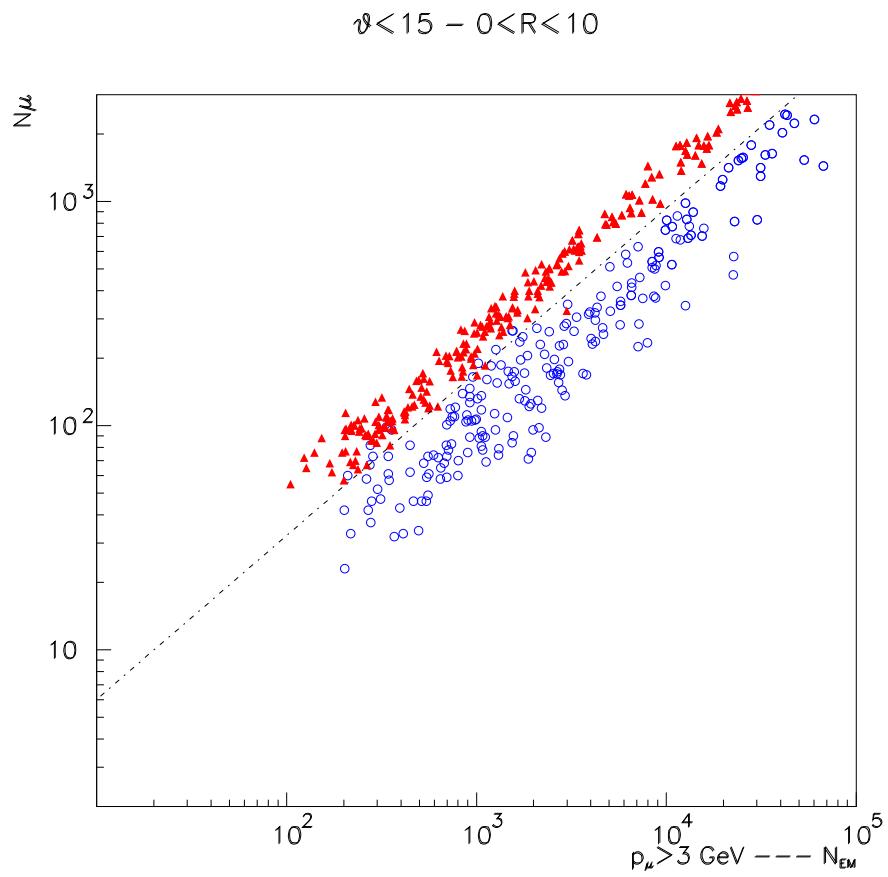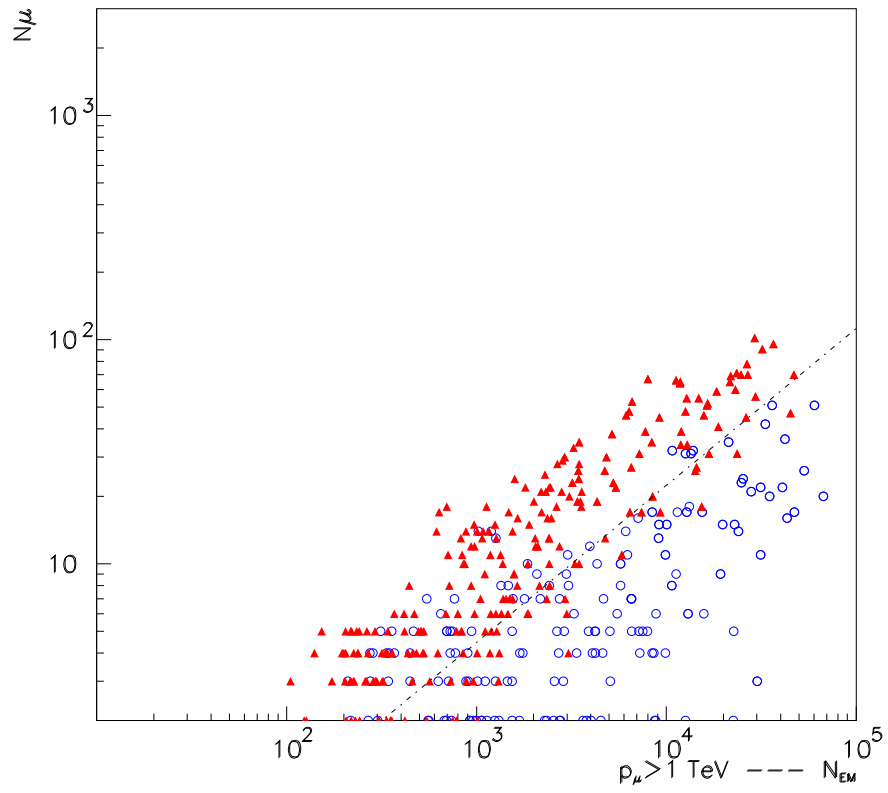
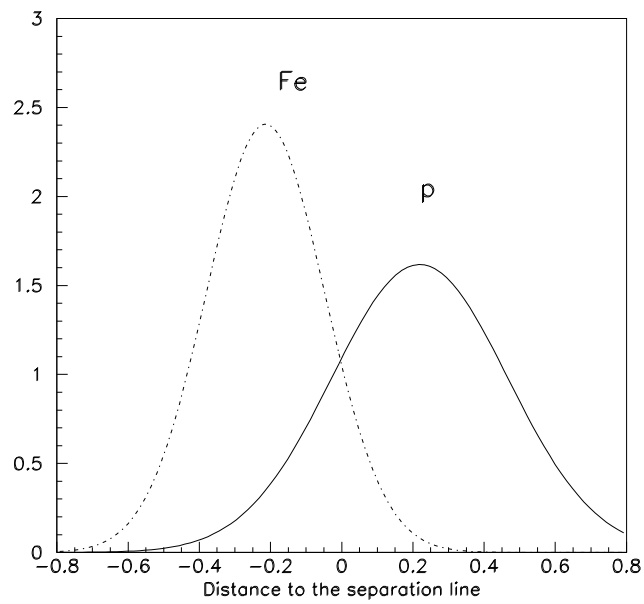Figure 3.2. The same as Fig. 3.1 for the "KASCADE" scenario with $p_\mu > 3$ GeV/c

Figure 3.3. The same as Fig. 3.1 for the "MACRO" scenario with $p_\mu > 1$ TeV/c

3.1.3 Precision of the Determination of Primary Particle Composition

We have studied the proton-iron separation for different muon multiplicities, i.e. primary energies, and for radial distances of the shower core from the center of the muon array of up to 20 m. The results are summarized in Tab. 3.2 where the peak positions and the widths of the Gaussian fits are given. There is no dramatic change in the quality of the separation. The separation variable is proportional to $\ln(A)$, where A is the atomic number of the primary particle. This relation allows us to determine the position of other elements such as He and O which are frequently used to describe the particle composition. The widths of these distributions are interpolated from the proton and iron cases for which detailed simulations were performed.

	$5 < N_\mu < 15$	$15 < N_\mu < 45$	$45 < N_\mu < 135$	$N_\mu > 135$
$0 < R < 10m$				
X_p	.182	.216	.211	.18
X_{Fe}	-.152	-.188	-.145	-.155
ΔX	0.334	0.405	0.357	0.335
σ_p	.219	.176	.174	.119
σ_{Fe}	.142	.119	.086	.071
$10 < R < 15m$				
X_p	.217	.177	.168	.15
X_{Fe}	-.255	-.2435	-.1788	-.186
ΔX	0.472	0.42	0.347	0.336
σ_p	.21	.2	.11	.11
σ_{Fe}	.16	.126	.097	.075
$15 < R < 20m$				
X_p	.197	.1966	.1924	.143
X_{Fe}	-.286	-.26	-.2	-.156
ΔX	0.483	0.456	0.392	0.299
σ_p	.22	.21	.1144	.113
σ_{Fe}	.14	.128	.0754	.068

$$X_{"He"} = X_p - \Delta X/3$$

$$X_{"O"} = X_{Fe} + \Delta X/3$$

$$\sigma_{"He"} = \sigma_p - \Delta\sigma/3$$

$$\sigma_{"O"} = \sigma_{Fe} + \Delta\sigma/3$$

Table 3.2. The position of the p and Fe curves in the separation variable and their standard deviation for different muon multiplicities and radial distances of the shower core to the muon array center. The formulas for the interpolation to He and O are given below the table.

With this knowledge, it is possible to perform a simulated analysis of particle composition models. The JACEE experiment has measured the particle composition at energies below 10^{14} eV and Swordy has predicted how this composition should change with energy. We used the individual fractions for p, He, O, and Fe as an input and generated 6000 events for each composition model using the separation curves described above, and assuming the muon multiplicities to be in the interval 45-135. We then fit to determine the element composition and the errors

from the simulated distributions. Fig. 3.4 shows an example of such a simulation together with the fits of the individual elements.The results are summarized in Tab. 3.3. The calculated compositions agree well with the input, with errors of the order of $\sim$ 1-2 %.
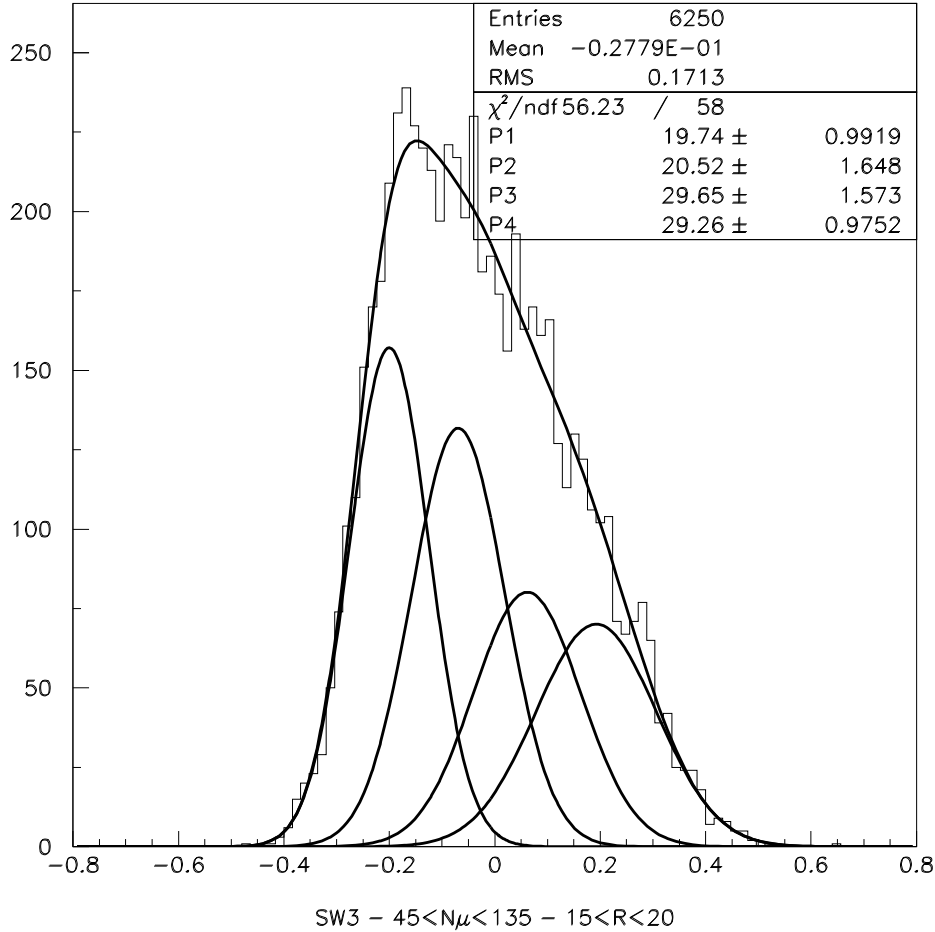

Entries	6250	
Mean	$-0.2779E-01$	
RMS	0.1713	
χ^2/ndf 56.23	/ 58	
P1	$19.74 \pm$	0.9919
P2	$20.52 \pm$	1.648
P3	$29.65 \pm$	1.573
P4	$29.26 \pm$	0.9752

SW3 $-$ 45$<$N$\mu<$135 $-$ 15$<$R$<$20

Figure 3.4. A simulated separation distribution with the primary particle composition of Swordy3 (see Tab. 3.3). The p,He,O and Fe curves, normalized to their individual fractions are also shown.

Often the variable $< \ln(A) >$ is plotted to characterize the change of the particle composition with energy. We have determined this value in two ways: first, from the individual element fractions and second, from the average of the separation distribution. These two values are also compared with the input value in Tab. 3.3. The $< \ln(A) >$ determination from the individually fitted fractions agree well with the input values, while the average determination is systematically lower by $\sim$ 3-4%.

Fig. 3.5 demonstrates what we would expect if the particle composition would change à la Swordy over the energy range of 5 10^{14} - 5 10^{16} eV. A clear change would be observed with increasing energy.

Table 3.3.

	p %	He %	O %	Fe %	$<lnA>_{in}$	$<lnA>_{fit}$	$<lnA>_{ave}$
JACEE in	24	31	33	12	1.827		
out	24.24 ± 1.10	30.75 ± 1.80	32.8 ± 1.5	11.36 ± 0.72		1.793	1.77 ± 0.02
Swordy1 in	35	28	24	13	1.577		
out	33.99 ± 1.24	27.52 ± 1.87	26.0 ± 1.5	11.76 ± 0.71		1.576	1.545 ± 0.022
Swordy2 in	22	23	35	20	2.094		
out	21.35 ± 1.0	22.79 ± 1.70	35.41 ± 1.59	19.04 ± 0.86		2.064	2.031 ± 0.022
Swordy3 in	20	20	31	29	2.304		
out	19.74 ± 1.0	20.52 ± 1.65	29.65 ± 1.57	29.26 ± 0.97		2.284	2.259 ± 0.022

Chemical composition, measured by the JACEE experiment at $E < 10^{14}$ eV and the change with energy à la Swordy. (Swordy1: $10^{14} < E < 3 \cdot 10^{15}$ eV; Swordy2: $3 \cdot 10^{15} < E < 10^{16}$ eV; Swordy3: $10^{16} < E < 10^{17}$ eV). The refitted values for a statistics of 6000 events are also given.
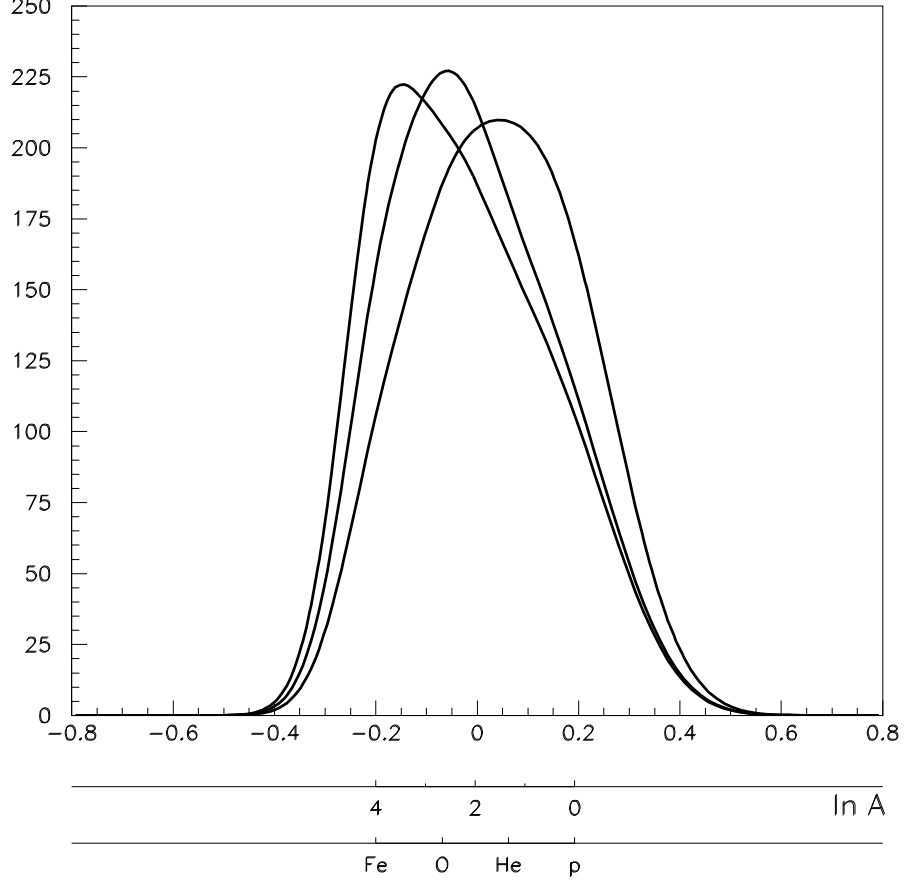
Figure 3.5. The expected separation distributions for Swordy 1-3 indicating the expected change over the CORAL energy range.
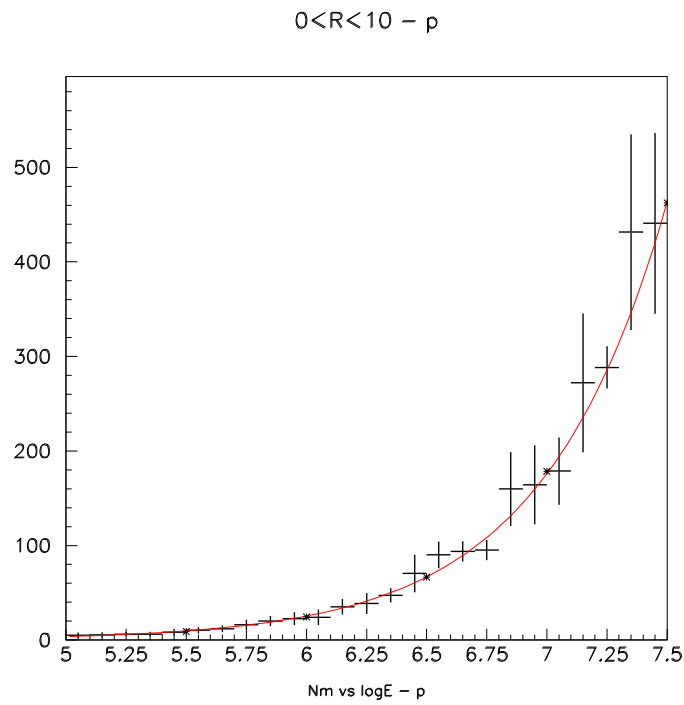

Figure 3.6. Energy calibration with muons. Number of muons in the detector for shower distances up to 10 m versus the primary energy.

14

3.1.4 Systematic Errors

As noted above, CORAL will be able to determine the primary particle composition with very small statistical errors, much smaller than the current uncertainty in the particle composition. This of course raises the question of systematic errors. CORAL is in a unique position to reduce these because of its ability to use several methods to discriminate between different types of cosmic ray primaries on an event-by-event basis, beyond those available to other experiments. We now discuss some of the relevant issues.
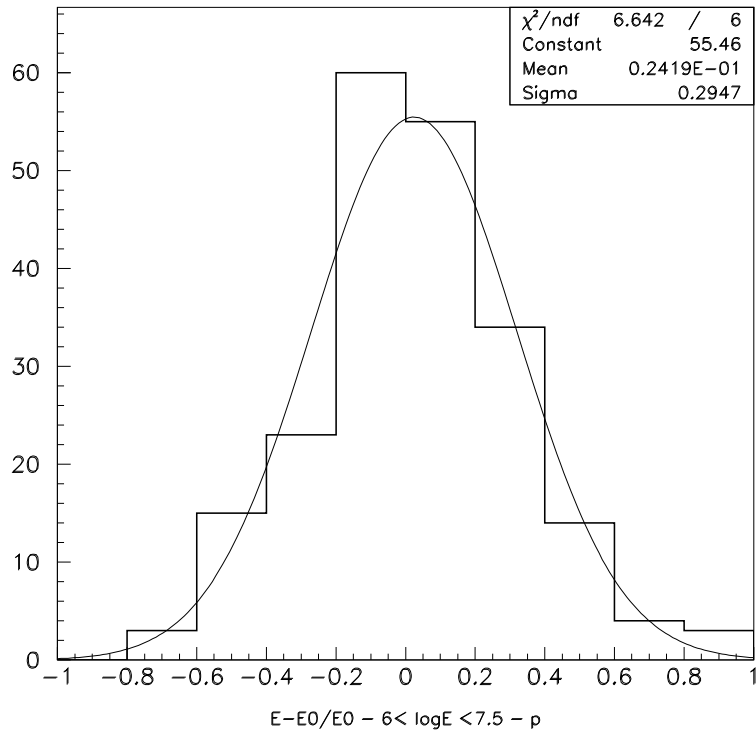
Because of the steep energy spectrum of the primaries, a precise energy determination is vital in order to minimize systematic effects on the particle composition. The energy determination should be independent of the particle type; this is almost the case if the energy is determined from the central muon density. Fig. 3.6 shows the calibration curve and Figs 3.7 the energy resolution for iron and proton primaries. A resolution between 20 and 30 % can be obtained depending on energy and improving with heavier primaries.

The dominant problem in the determination of the primary composition is the control of systematic effects which arise from the unknown forward particle production. Several input models have been tried but there remains an uncertainty between these models and the primary particle determination. We have compared four models: QGSJET, SIBYLL 2.1, DPMJET 2.5 and neXus 2 (thanks to D. Heck from Karlsruhe, who provided us with these simulations). The radial dependence of the muon density for these four models is given in Figs. 3.8- 3.10 for proton and iron induced showers and for three different momentum cut-offs (3, 70 and 1000 GeV). Except for the highest cut-off, where the QGSJET model differs from the others, the agreement between the models is remarkable, being best at the CORAL momentum cut-off. For our simulations we have chosen the QGSJET model which has successfully confronted a variety of experimental results.

To better understand and to reduce systematic effects, we have performed an almost independent analysis for the particle composition determination that is entirely based on the radial distributions of the muons. As can be deduced from Fig. 3.11, the radial distributions differ considerably for heavy and light primary particles. The flatter distribution for iron induced showers is a basic effect arising from the earlier development of the shower in the atmoshere and from the increased hadron multiplicity. For our analysis, the radial range up to 40 m is relevant. Comparing the different muon momentum cut-offs the separation between the curves is getting larger with higher momenta. But at the same time the muon density, and hence the statistics, is decreasing fast. These two balancing effects lead to an optimal separation around the CORAL cut-off. We have performed a detailed analysis calculating, for a given shower core position, the muon number in each chamber and comparing it with the proton and iron hypothesis. The result is summarized in the two-dimensional plot (Fig. 3.12) where the likelihoods for the two assumptions are plotted. We can obtain a discrimination between proton and iron primaries which is better than 80% using only the radial distribution. This is an important check of the systematics of the electron-muon analysis.

A combined analysis using both the electron-muon analysis and the radial muon distribution should suffer less from systematic effects. The ability to determine the effective height of the primary interaction will also be a powerful tool in untangling various possible systematic effects. Finally, it is important to note that CORAL will overlap at low energies with ACCESS, an experiment at the International Space Station that is being designed to study the primary cosmic ray composition by direct observation.

0<R<10 − p

χ^2/ndf	6.642 / 6
Constant	55.46
Mean	0.2419E−01
Sigma	0.2947

E−E0/E0 − 6< logE <7.5 − p

0<R<10 − Fe

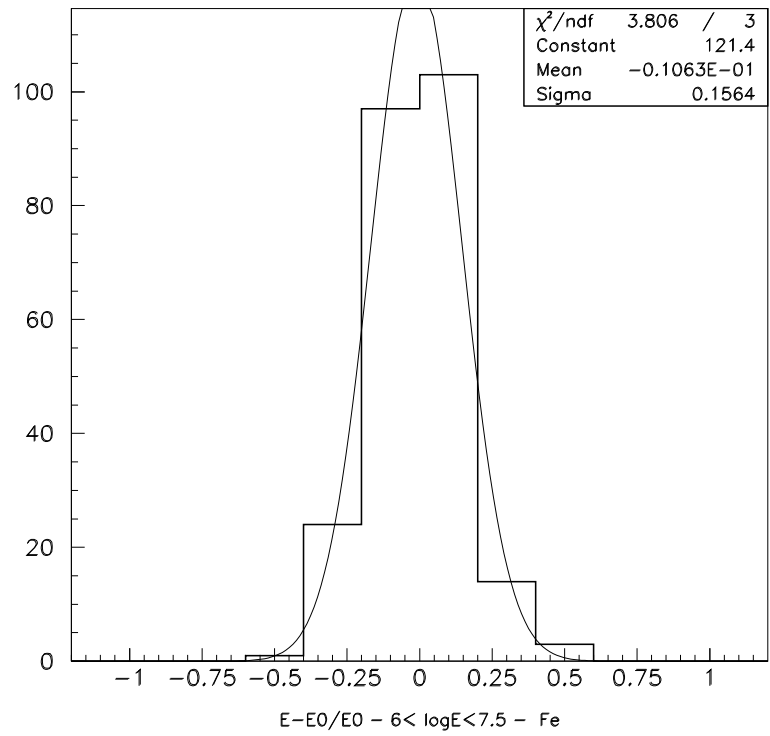| χ^2/ndf | 3.806 / 3 |
Constant	121.4
Mean	−0.1063E−01
Sigma	0.1564

E−E0/E0 − 6< logE <7.5 − Fe

Figure 3.7. Energy resolution curves for p and Fe in the energy interval $10^{15} − 3 \cdot 10^{16}$ eV.
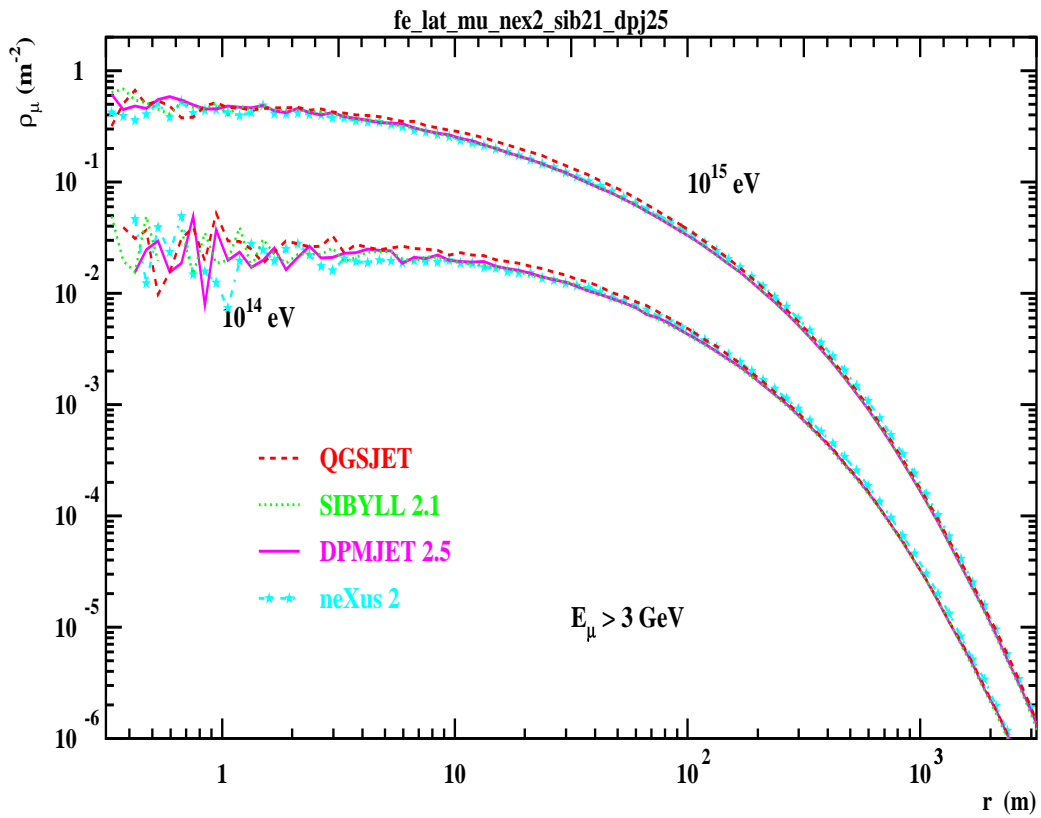
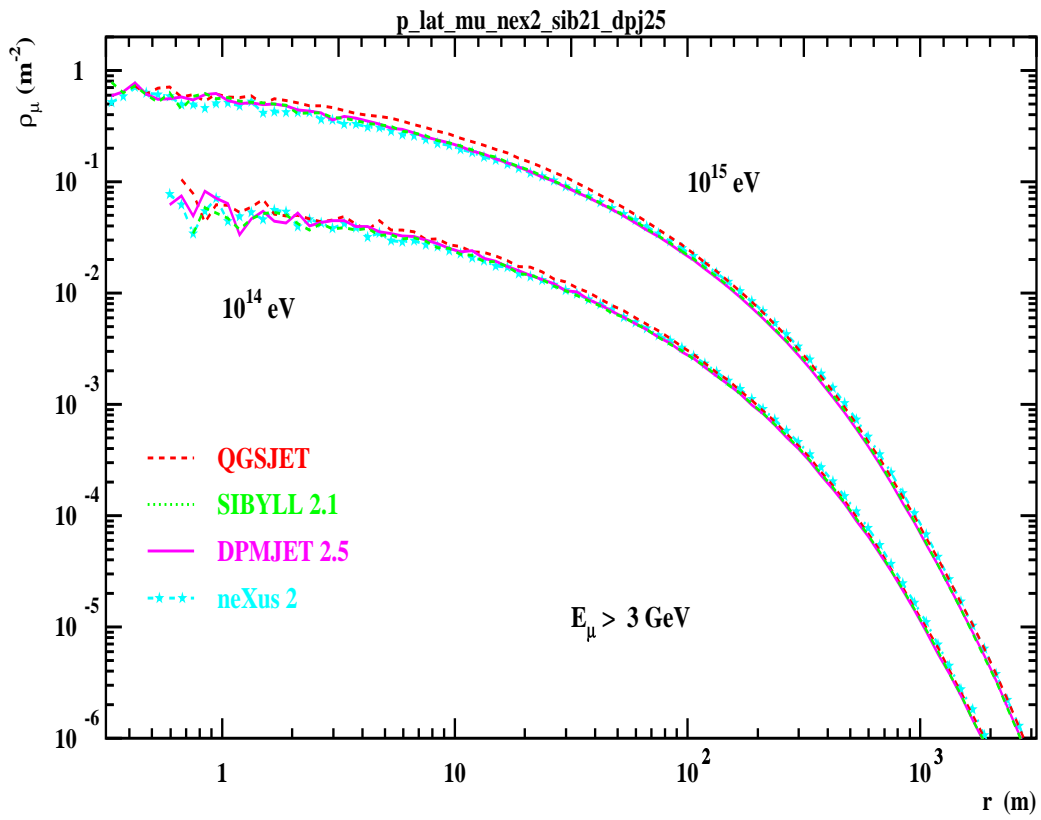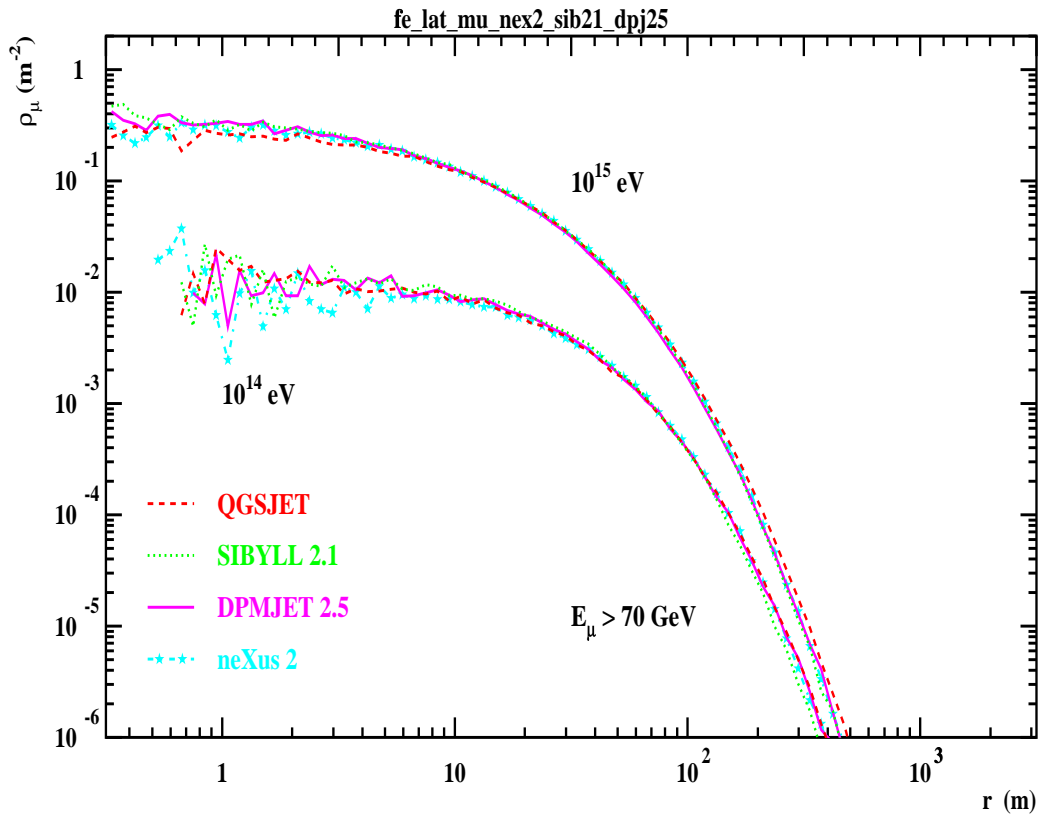*Figure 3.8. The radial dependence of the muon density for $E_\mu > 3$ GeV for p and Fe and for four input models.*
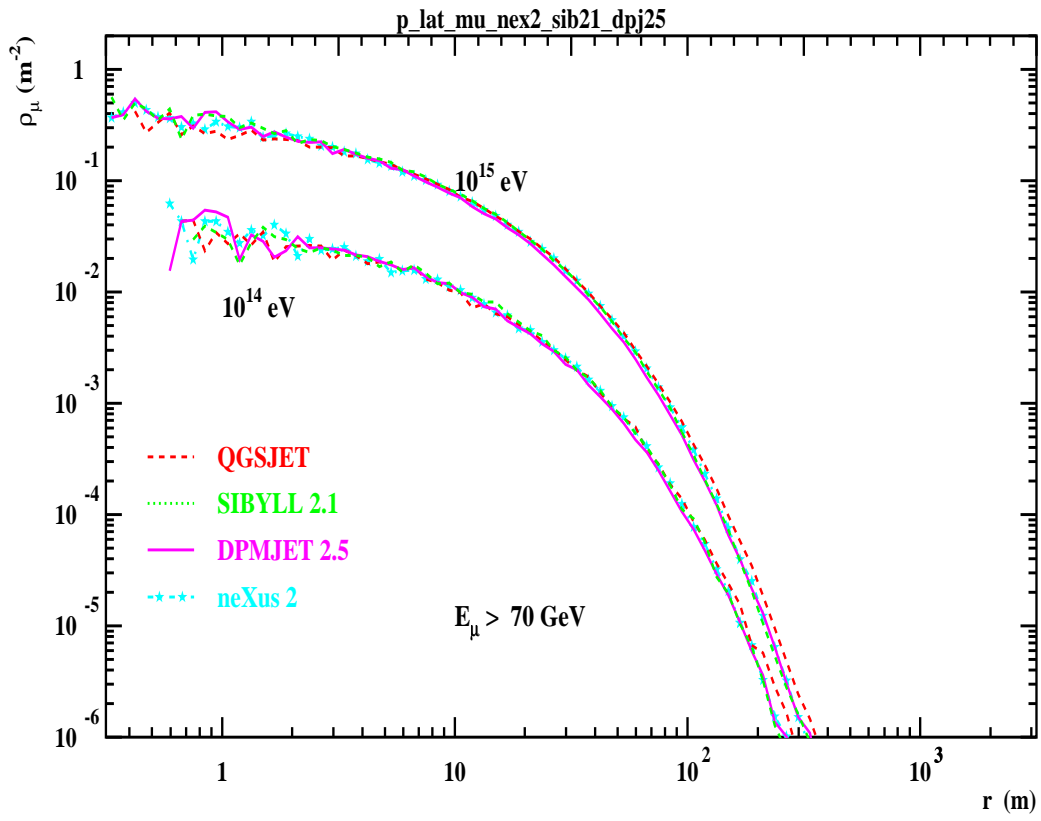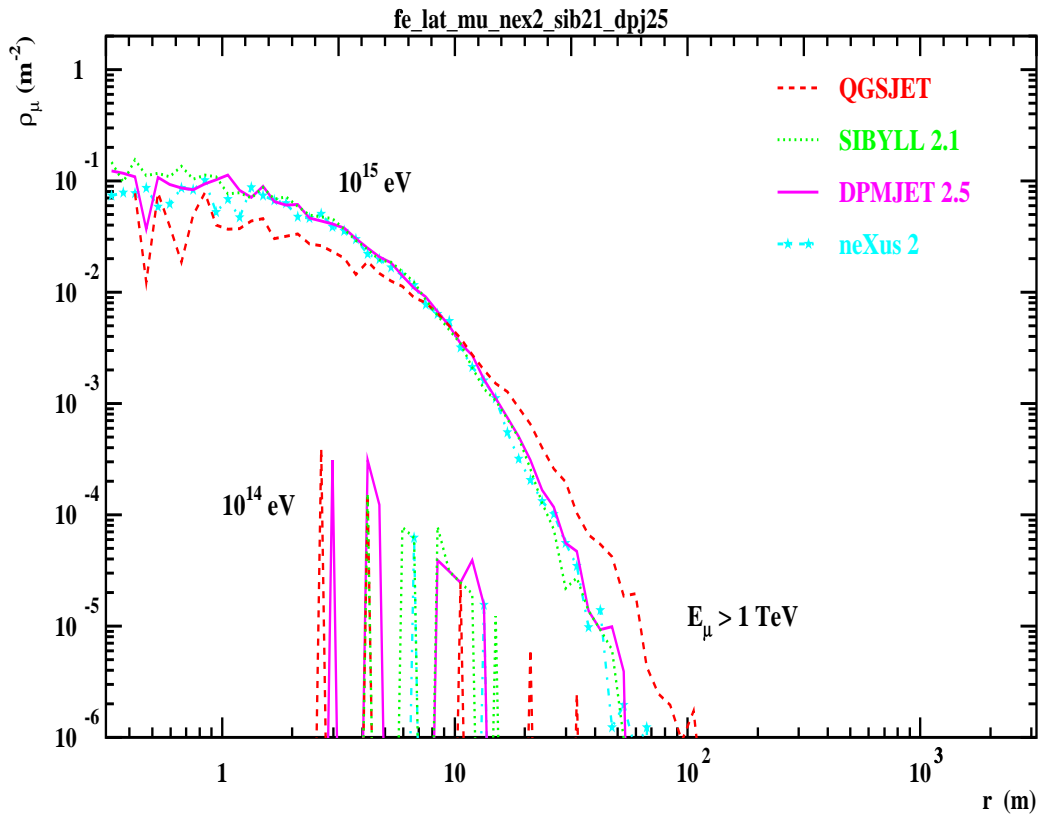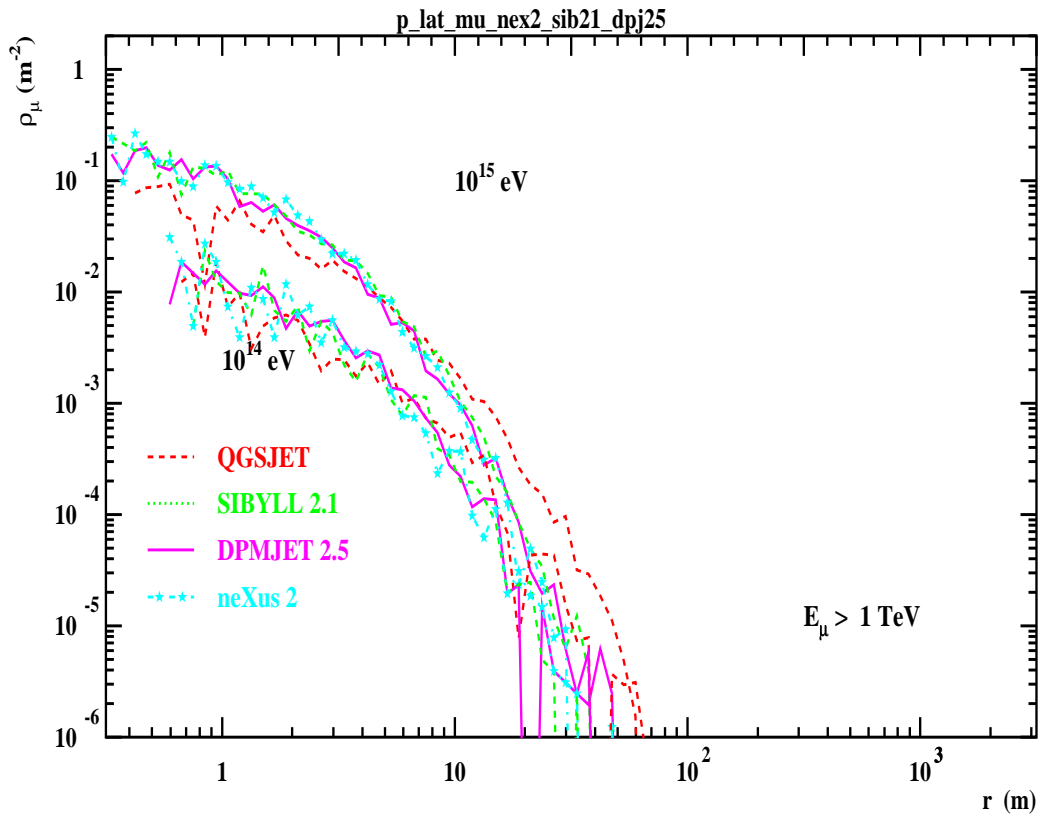
Figure 3.9. As Fig. 3.8 for $E_\mu > 70$ GeV

Figure 3.10. As Fig. 3.8 for $E_\mu > 1$ TeV
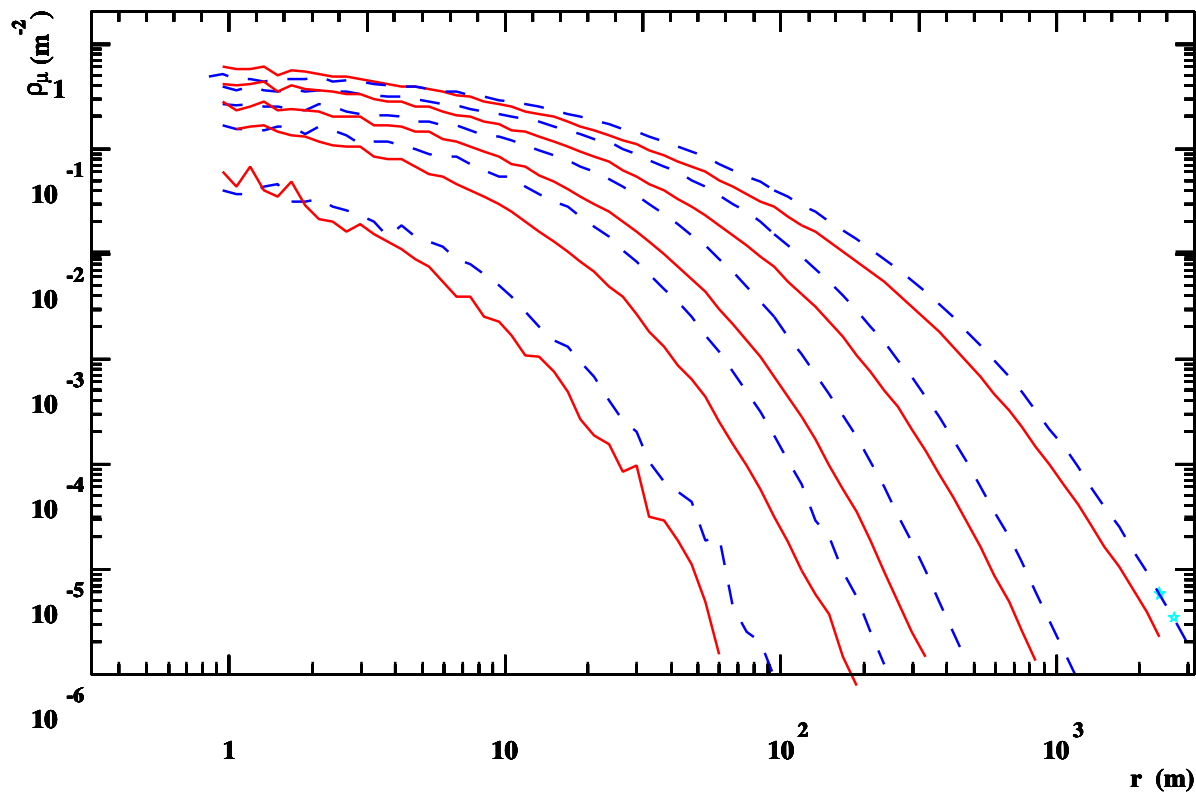
Figure 3.11. The radial dependence of the muon density for Fe (dashed) and p (solid) induced showers for different muon momentum cut-offs (from the top: $p_\mu > 3, 20, 70, 200, 1000$ GeV/c).
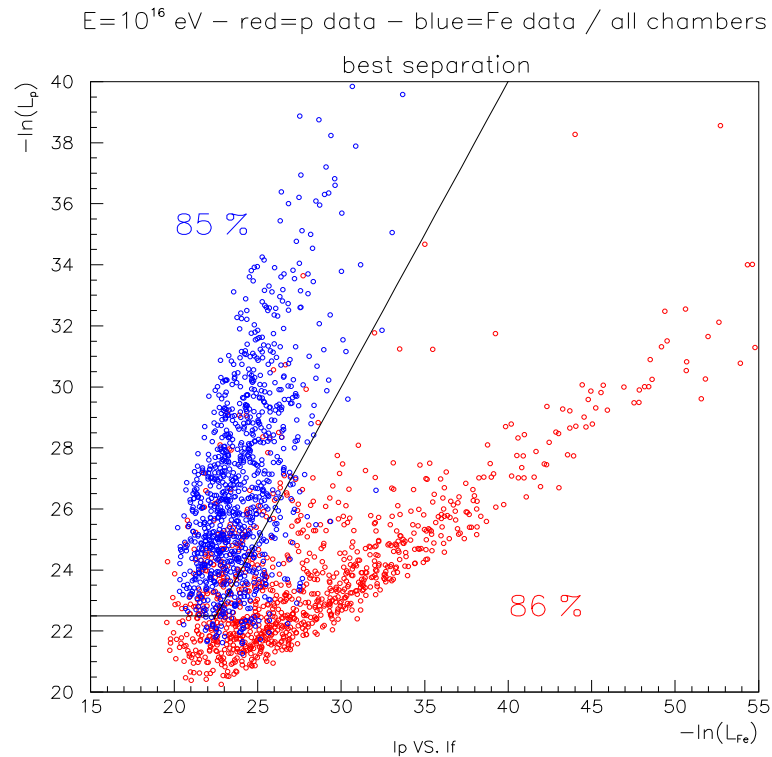

Figure 3.12. $-\ln(L_p)$ vs $-\ln(L_{fe})$, where $L_{p(fe)}$ is the likelihood, for a proton (iron) sample. The fraction of correctly identified events refer to the cuts shown in the plots.

3.2 Determination of the Shower Height

The determination of the shower height provides an additional tool that can be used to discriminate between heavy and light primaries. Fe induced showers typically begin higher in the atmosphere ($\sim$ 30 km) than proton showers ($\sim$ 20 km). Since a large fraction of the 70 GeV muons are coming from approximately the first four interactions the effective height is reduced to about 5 - 15 km, depending on the primary particle. Furthermore, muons arising from large hadron densities in the first interactions (see e.g. DCC) will start higher in the atmosphere. A height determination will therefore help to characterise these processes, particularly since large muon densities will enable a better height determination.

If a muon bundle with some 500 particles hits near the center of the underground muon array, the direction of the shower axis can be determined with a precision of $\sim$ 0.2 mrad by averaging over all muon directions. The multiple scattering of the individual muons follows a Gauss distribution with a width of $\sim$ 2 mrad and large tails. This was experimentally verified with the five highest multiplicity events observed with the ALEPH detector (see Sec. 3.3).

To demonstrate the capability of the height determination we have chosen three different heights (10, 20 and 30 km) and have tracked the muons to the underground array on straight lines. We then applied a multiple scattering error of 2 and 3 mrad accounting for the multiple scattering and refitted the vertex. A typical χ^2 distribution of the fit is given in Fig. 3.13.
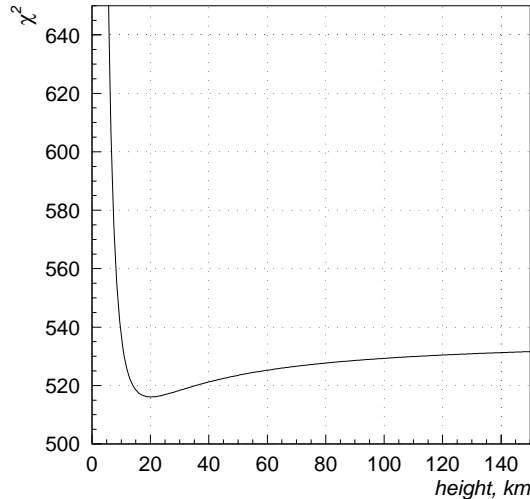

Figure 3.13. χ^2 as a function of the interaction height for 500 muons coming from a height of 20 km.

The reconstructed height distributions are shown in Figs 3.14 for two muon multiplicities and two multiple scattering errors.

The curves are well separated. If all muons would come from a fixed height, CORAL will be able to determine this height with a typical precision of a few km. We have also reconstructed the effective height of proton- and iron induced showers from the muons of the complete shower simulation, including tracking through the 140 m overburden. Due to the fact that most of the muons are not coming from the first interaction, the effective shower height is now lower, but there is still discrimination between light and heavy primaries. Figs. 3.15 show the height distributions for proton- and iron induced showers of 10^{16} eV energy for two shower core positions.

It is worth mentioning that the muon production height increases almost linearly with the
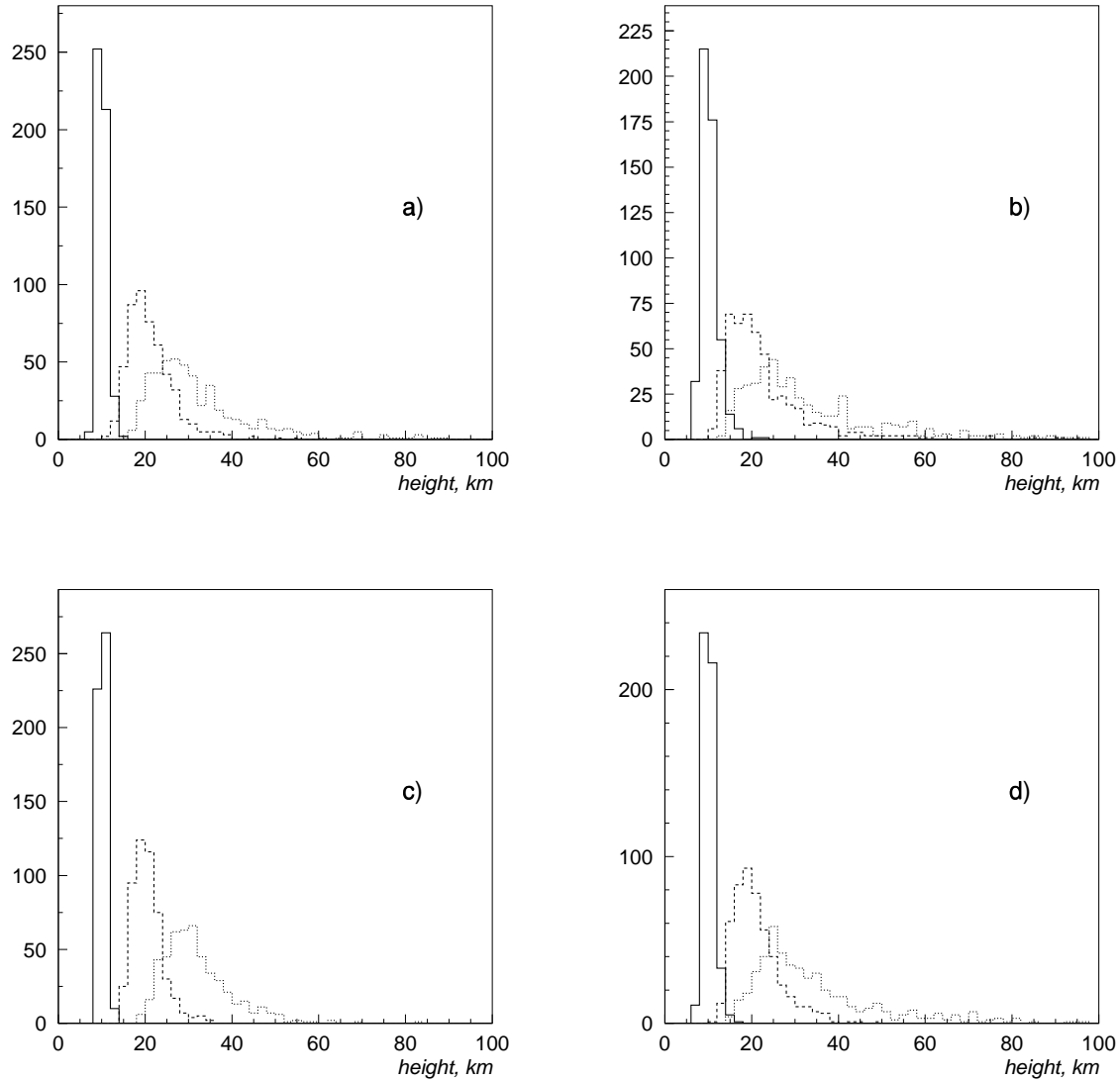
Figure 3.14. Distributions of the reconstructed interaction heights for different cases: a) 250 muons and track scattering error of 2 mrad, b) 250 muons and error of 3 mrad, c) 500 muons and 2 mrad, d) 500 muons and 3 mrad. Solid line for 10 km interaction height, dashed for 20, dotted for 30.

muon momentum. By cutting on small multiple scattering angles in the tangential plane and determining the scatter angle in the radial plane we will select high energy muons coming predominantly from the first interactions higher up in the atmosphere. Experiments with low momentum cut-offs are dominated by muons originating late in the cascade, close above them. These muons obscure much of the information about the primary interaction.

Figure 3.15. Reconstructed heights for proton (dashed) and iron (solid) induced showers for two locations of the shower core (0 and 5 m from the muon array center)
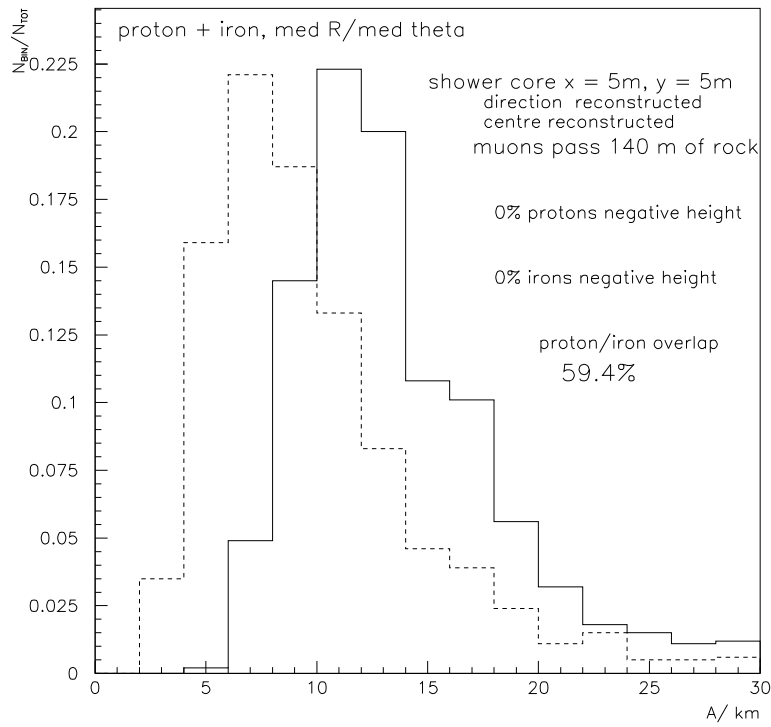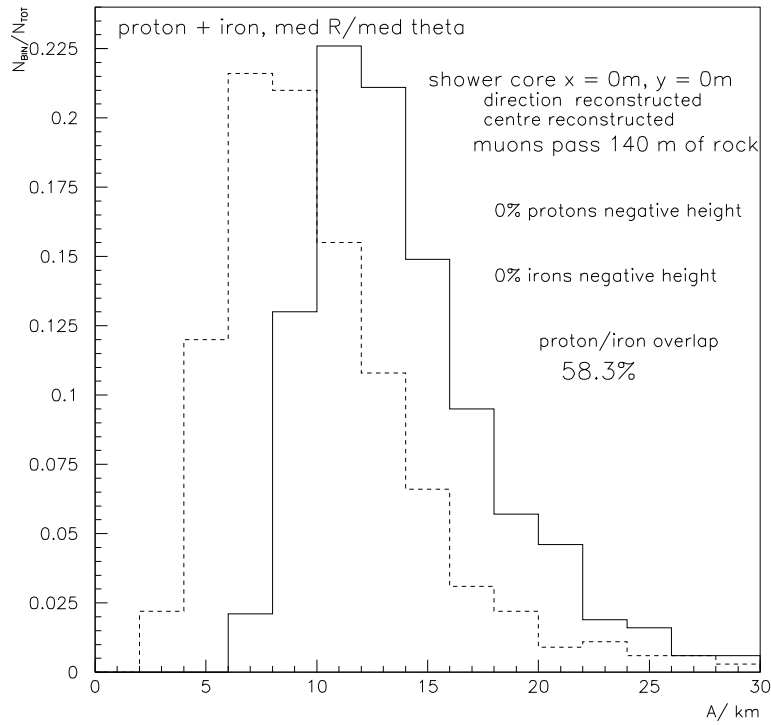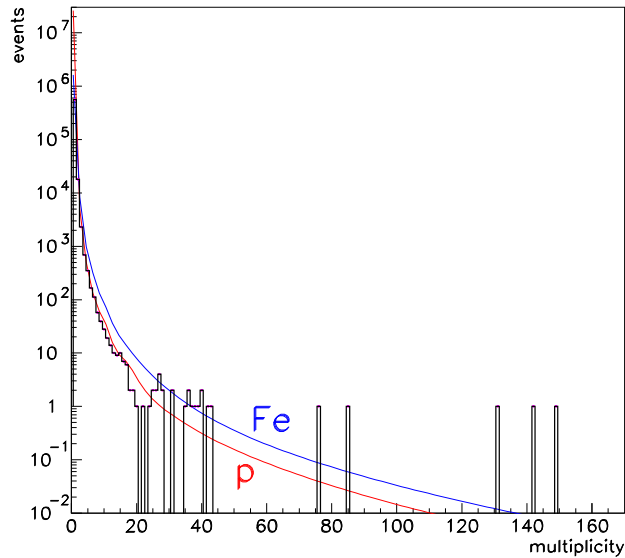
Figure 3.16. Multiplicity distribution of muons in the TPC compared to CORSIKA simulations for p and Fe as primary particle. The highest multiplicity event has twice the particle density (see Tab. 3.4)

3.3 Significance of the High Multiplicity Excess Seen in the ALEPH Detector

Fig. 3.3 shows the measured distribution of the muon multiplicity in the TPC together with the QGSJET CORSIKA simulation for proton and iron primary particles, absolutely normalized to the effective running time. Up to a multiplicity of 20, the proton curve describes the observed data well over several orders of magnitude, indicating that the primary spectrum is dominated by light elements at energies corresponding to these multiplicities. The discrepancy in the single muon rate is due to the low efficiency of the LEP triggers for single muons; this efficiency approaches 100% only if there are more than two muons in the TPC. At larger multiplicities there is evidence for a transition to the iron curve.

While the simulation agrees with the data over a wide multiplicity range, it fails to describe the highest multiplicities, even under the assumption of a pure iron composition. This is better demonstrated with the integral distribution in Fig. 3.17, which is plotted on a log-log scale for shower zenith angles below and above 30°. It is worth noting that four of the five highest multiplicity events have zenith angles beyond 30°. Their zenith angle distribution differs considerably from the other high multiplicity events, as can be seen in Fig. 3.18.

Fig. 3.19 shows the distributions of track angles for the 5 highest multiplicity events in the non-bending plane, whereas Fig. 3.20 presents the angle in the non-bending plane as a function of the track momentum. One can see, that by selecting tracks with momenta above 100 GeV and within ± 20 mrad in bending and ± 10 mrad in non-bending planes, one can exclude most of the significantly scattered tracks. The remaining tracks (Fig. 3.21) were used to evaluate the interaction height, which is included in Tab. 3.4.

Tab. 3.4 summarizes the characteristics of the five highest multiplicity events. An estimate of the primary energy was made under the assumption that the shower center is in the TPC. The energy was calculated assuming proton-induced showers and would be 30% lower for iron. If the shower cores were further away, the energies would be even larger. For comparison, Tab. 3.5 presents the expected numbers of showers for different energy cuts extracted from the all-particle spectrum.

24
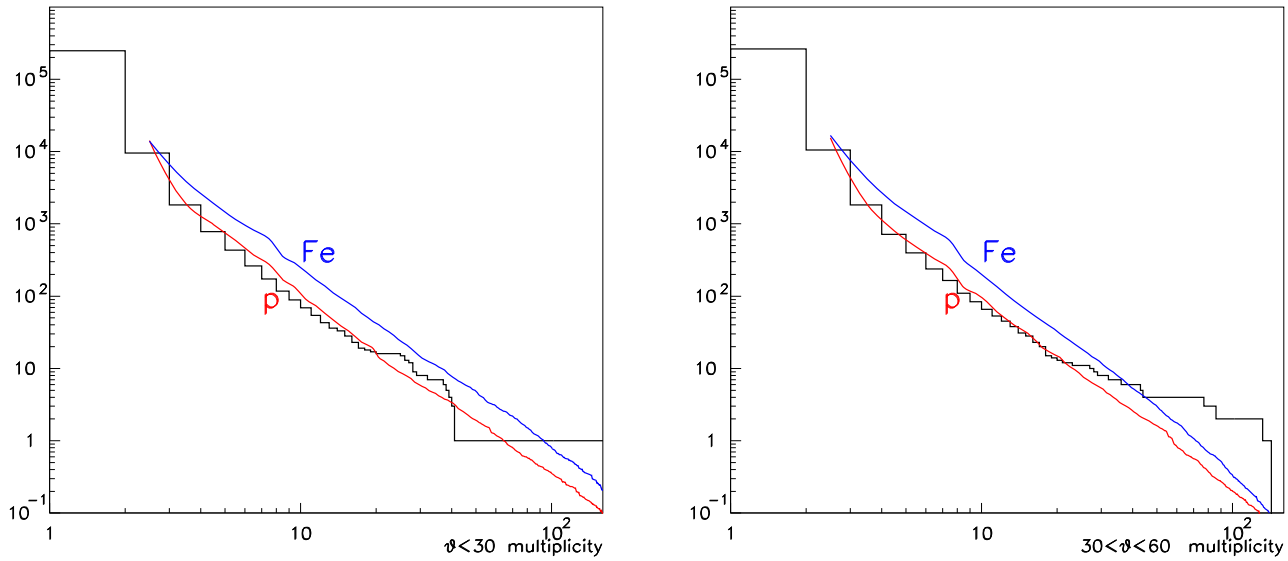
Figure 3.17. Integral multiplicity distributions of muons in the TPC for two different zenith angle intervals ($\theta < 30^o$ and $30^o < \theta < 60^o$) compared to CORSIKA simulations for p and Fe. Power law fits of the M.C. curves yield an exponent of about -1.8.
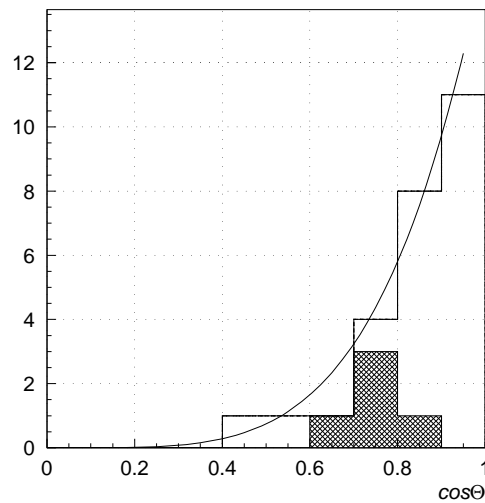
Figure 3.18. Zenith angle distribution for events with track multiplicity $19 \leq N_\mu \leq 50$ compared with CORSIKA prediction (line). The highest multiplicity events ($N_\mu > 50$) are shown as a hatched histogram.
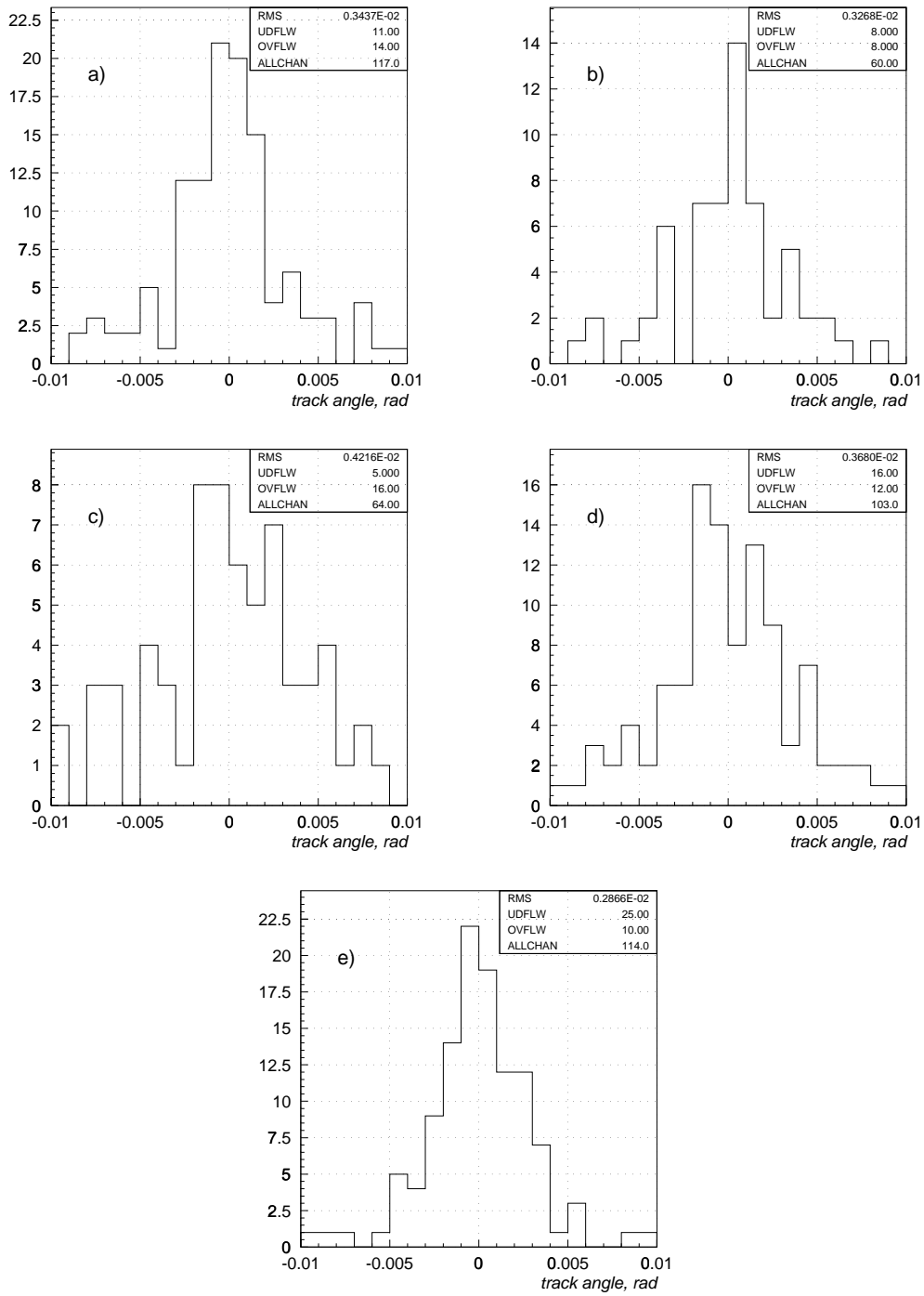
Figure 3.19. Track angles in non-bending plane: a) event with 142 tracks, b) with 76 tracks, c) with 85 tracks, d) with 131 tracks, e) with 149 track.
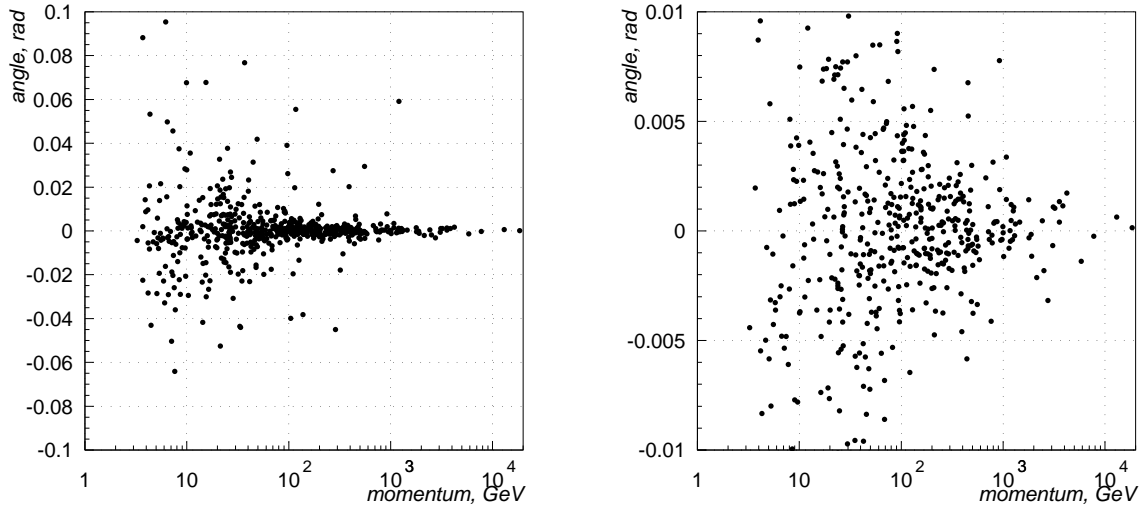
Figure 3.20. Track angle in non-bending plane as a function of reconstructed momentum (note the different vertical scales).

Number of tracks	Muon density, m^{-2}	Zenith angle, ^{o}	Primary energy, eV	Interaction height, km
76	4.8	40.6	$3.0 \cdot 10^{16}$	$7.8^{+\infty}_{-5.3}$
85	5.3	38.4	$3.0 \cdot 10^{16}$	$39.3^{+\infty}_{-36.3}$
142	8.9	40.5	$5.7 \cdot 10^{16}$	$3.7^{+152.6}_{-1.8}$
149	18.6	27.3	$7.4 \cdot 10^{16}$	$2.7^{+\infty}_{-1.4}$
131	8.2	48.0	$8.2 \cdot 10^{16}$	$3.5^{+\infty}_{-1.8}$

Table 3.4. Characteristics of the highest multiplicity events. The primary energy was estimated by assuming the shower centre to be close to the TPC and taking into account the zenith angle.

Energy cut, eV	Expected number of events
$1. \cdot 10^{16}$	1.59
$3. \cdot 10^{16}$	0.17
$6. \cdot 10^{16}$	0.043

Table 3.5. Expected number of events.

27
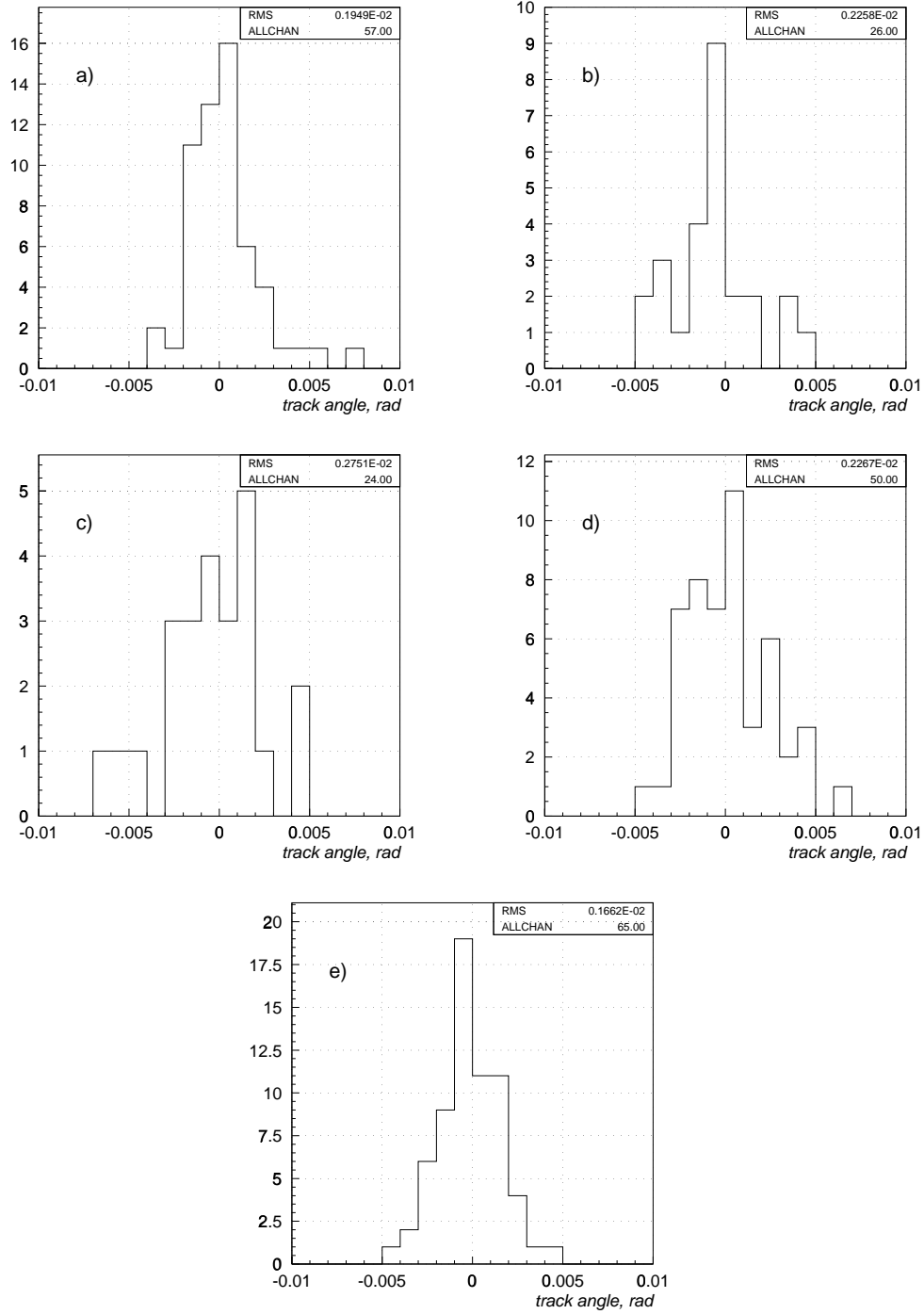
Figure 3.21. The same as in Fig. 3.19 for the following cuts: track momentum greater than 100 GeV, angle in non-bending plane below 10 mrad and in bending plane below 20 mrad.

28

3.4 Sensitivity to Disoriented Chiral Condensates and other exotic physics

A unique strength of CORAL will be the ability to track and count muons in and near the cores of showers. Taken alone, this permits CORAL to undertake the study of possible anomalies in the muon multiplicity distribution. An important example of such an anomaly is that reported in the ALEPH cosmic ray data and discussed above.

The CORAL underground muon array will, however, operate in conjunction with a surface array sensitive to the electromagnetic component of the air showers. This will permit detailed studies of the joint distribution of the muon and electromagnetic components of the air showers. Since the muons arise dominantly from decays of charged pions, and the electromagnetic component is initiated by neutrals, these measurements reflect the joint charged-neutral multiplicity distributions resulting from the primary collision. Of course, the particles observed by CORAL result from the convolution of these primary distributions by the subsequent evolution of the air shower. It is the purpose of this subsection to discuss the degree to which CORAL is nevertheless sensitive to new physics resulting in anomalies in the joint multiplicity distributions.

A wide variety of such anomalies relevant to CORAL have been reported in the cosmic ray literature or suggested on the basis of theoretical considerations. The FELIX LoI reviews many examples of each [2]. For our present purposes, we will consider a single type, illustrating many of the features relevant to the general discussion of possible anomalies: Disoriented Chiral Condensates (DCC) and the possibly related reports of "Centauro" or "anti-Centauro" events in cosmic rays[3].

The possibility of disoriented chiral condensates arises from theoretical suggestions that pieces of strong-interaction vacuum with an unconventional orientation of the chiral order parameter may be produced in high energy collisions. This disoriented chiral condensate (DCC) then decays via coherent radiation of pions with the same chiral orientation.

The primary signature of this mechanism is the presence of large

event-by-event fluctuations in the fraction, f, of produced pions that are neutral. Conventional mechanisms of particle production, including those used in standard Monte-Carlo simulations, predict that the partition of pions into charged and neutral species is governed by a binomial distribution which, in the limit of large multiplicity, leads to a sharp value of f. On the other hand, for the decay of a pure DCC state, the distribution of the neutral fraction is very different, following an inverse square-root law in the limit of large multiplicity.

In addition to the hallmark signature based on anomalous charged-neutral fluctuations, there are also suggestions that pions arising from the decay of DCC may be characterized by low transverse momentum, and may be localized in regions of phase space. These uncertainties complicate the search for DCC at accelerators, where most modern detectors are by design blind to low p_t particles. These considerations also make the use of Monte-Carlo simulations comparatively less useful. Instead, recent search strategies have exploited the fact that certain "robust observables" can be defined that are sensitive to the presence of DCC and are insensitive to most of the uncertainties; Monte-Carlo simulations have mainly been used to confirm the expected properties [4].

It has been suggested that DCC may provide an interpretation of the Centauro events originally seen by the Brazil-Japan collaboration in high-altitude emulsion chamber experiments. These are events in which a large number of hadrons are observed, along with little or no electromagnetic radiation [5]. These events are not particularly rare; the probability of production of a Centauro event in an interaction of one PeV or above is about 1%.

If Centauro events are signals of DCC production, then anti-Centauro events, in which large amounts of electromagnetic radiation are observed with little or no hadronic activity, should also be seen. Such events had not been reported at the time DCC was proposed on theoret-

ical grounds; there have been several reports since that time [6]. Indeed, both Centauro and anti-Centauro events now appear to be extreme cases of an admixture of events with a broad, anomalous charged-neutral distribution.

CORAL's search for anomalous charged-neutral fluctuations will exploit the formalism for robust observables which has been developed [4]. The extension to the actual observables measured by CORAL is in principle straightforward, and the relevant formalism has been outlined.

The key to CORAL's sensitivity is the fact, noted in the previous section, that pions of energies of ~ 100 GeV have a decay length comparable to the interaction length at the height of typical primary interactions, and are nicely matched to the CORAL muon energy threshold. Conversely, CORAL is not sensitive to low energy muons arising from late stages of the shower.

While muons arising from the decay of pions produced in the primary interaction will nevertheless only be a small fraction of the total number of muons seen in an event, this fraction is large enough, the total number of muons observed is large enough, and the total number of events will be large enough that CORAL will easily be sensitive to the presence of DCC (or Centauro events) at the suggested level.

While the utility of this approach is not in doubt, Monte-Carlo simulations will, nevertheless be useful. This will require extensive simulation of these (anomalous) cosmic ray air showers, and will be computing-intensive. This work will, however, proceed in parallel with the CORAL experiment.

The CORAL search strategy is not confined to the use of such robust observables. For example, pure anti-Centauro events will have a striking signature: an electromagnetic shower visible in the surface array, with little or no activity in the underground muon chambers. These events will be distinguished from conventional electromagnetic showers induced by gamma rays by the broader radial distribution characteristic of hadronically induced events. Similarly, the very sharp cutoff of the distribution of events arising from Fe primaries will permit a direct search for Centauro-like events.

In this context, it will be very interesting to examine the electromagnetic structure of events such as those seen in the ALEPH detector. If the electromagnetic component is normal, then these events represent one kind of anomaly, as discussed above. On the other hand, it is possible that the electromagnetic component is suppressed, in which case the energy estimates given above will be too high, but in this case the events will represent a Centauro-like anomaly.

In all of these searches for anomalies, CORAL's ability to discriminate between events based on the determination of the effective height of the event will provide an additional powerful constraint on the consistency of the interpretation of putative anomalies.

It should be noted that studies of the joint multiplicity distribution or phase space structure are in their comparative infancy, even in the domain of accelerator physics. This is even more true in the case of Cosmic Ray physics. The variety of possible anomalies reported in cosmic rays or suggested by theoretical considerations, combined with CORAL's unique strenghts, suggest that the discovery potential is very high indeed.

3.5 Angular Resolution of the Surface Array

The zenith angle of an incoming shower can be determined using timing information from the various counters of the surface array. The timing information are matched to the fluctuations of the shower front; typical time resolutions are ~ 1 nsec. Other experiments have generally been able to determine the zenith angle of the shower axis to within about 5 mrad using this technique. Using better timing information, the KASCADE experiment has recently claimed an improved resolution of ~ 2 mrad.

As a comparison, the shower axis can be determined with a precision of ~ 0.2 mrad from

muons hitting the underground muon array. The surface array does not, therefore provide a significant improvement in the height determination. The surface array is, however, vital for the extrapolation of the shower core from the surface array to the underground array if the core is far away from the center of the underground muon array.

3.6 Optimal Character of the Proposed Design

3.6.1 The surface Air Shower Array

The size of the surface array is determined by several considerations:

- For incident zenith angles above about 25°, the electromagnetic component of the shower starts to be more absorbed, leading to significant reductions in the precision with which the shower energy can be determined.
- The surface array is located 140 m above the underground muon array, and is centered on it. Since we are interested in showers with cores passing through the underground array and with zenith angles of less than 25°, this means that we are interested in air showers whose core lies within 60 m of the center of the air shower array.
- The electromagnetic component of the air shower falls rapidly with radial distance from the shower core. Most of the electromagnetic energy is contained within 50 m; we have obtained good results using circles as small as 20 m.

Thus, the proposed surface array of area 200 x 200 m^2 is well matched to the goals of the experiment. It is also similar in size to other arrays already constructed, such as the one used by the KASCADE experiment. Note, however, that we have chosen a counter distance of 10 m, slightly smaller than that used in other experiments, permitting a better reconstruction of the shower axis and a more detailed understanding of the electromagnetic shower development.

3.6.2 The Underground Muon Array

The radial distribution of muons becomes steeper with increasing muon momentum. In our case, with a muon momentum threshold of 70 GeV, the muon density drops by an order of magnitude over a radial distance of 15 m from the shower core. The size of the underground muon array, 20 x 20 m^2, is thus well matched to the radial distribution of muons.

A larger underground muon array would surely increase statistics. This could be accomplished as an upgrade at a later stage of the experiment by placing some of the large OPAL muon chambers at some more distant locations in order to obtain additional information about the radial distributions.

For the present design it is important to note that we have placed a strong emphasis on the precise reconstruction of very dense muon showers. Thus we have placed 12 planes in one projection and 6 planes in the other on top of each other, rather than spreading the chambers over a larger area.

3.6.3 A Surface Muon Array?

A surface muon array would add little additional information at the cost of very significant complications. Even if such an array were included, it could not be used to improve tracking. Due to multiple scattering in the overburden, the underground muon tracks cannot be extrapolated with sufficient precision to match them with muons on the surface where the muon density is more than three times as large even under a 3 m Fe absorber. Nor are these extra muons, which dominantly arise from late stages of the shower development, either particularly interesting or useful. Further, in order to obtain a zenith angle acceptance comparable to that of the underground muon array matched with the surface air shower array, the area of a surface muon array would have to be increased by at least an order of magnitude.
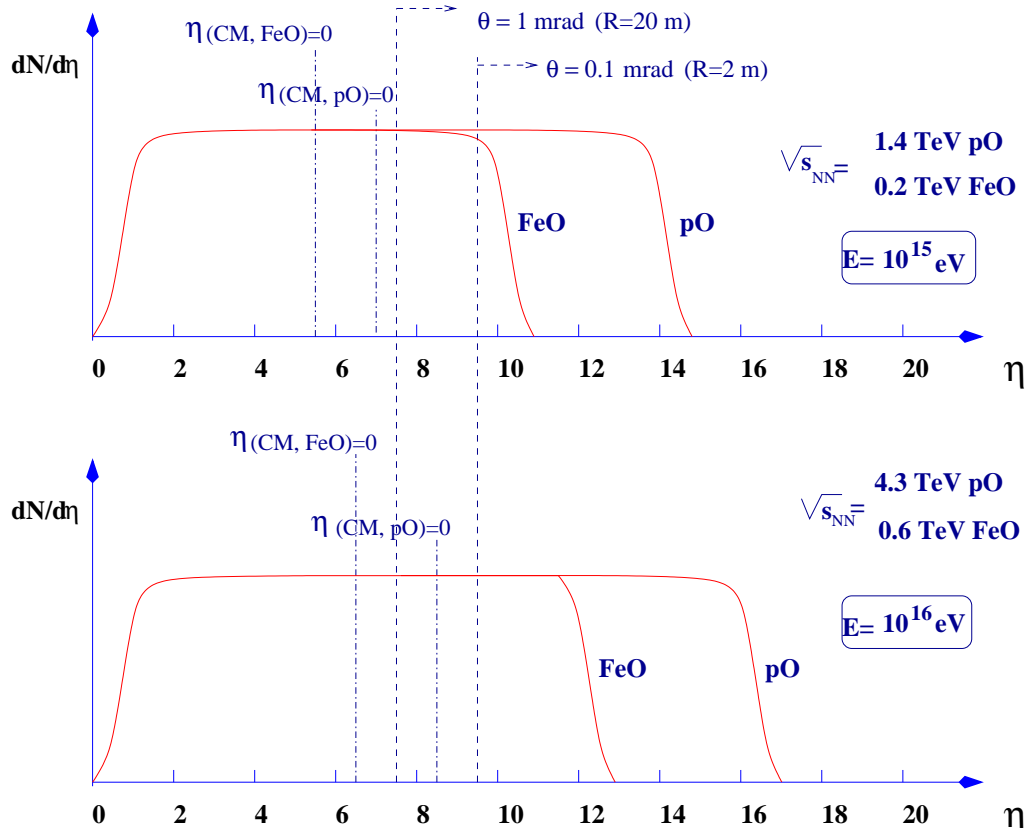
Figure 3.22. Schematic pseudorapidity distributions in the fixed target frame for p-O and Fe-O collisions.

3.7 Relationship to the LHC

The cosmic ray energy range accessible to CORAL overlaps with the LHC energy for heavy ion collisions. We expect more than 1000 events with energies above 10^{16} eV and shower cores close to the muon chambers. If new effects are observed with CORAL, it will be possible to check whether they are in the acceptance of the ALICE detector and can thus be confirmed. This will disentangle the inherent cosmic ray problem of whether the origin of an effect is due to the particle interaction or due to an unknown primary (the astrophysics connection).

CORAL will obviously detect the complete forward cone of the heavy ion fixed target interaction. Lorentz-boosting back into the center-of-mass system, the radial distances from the shower axis can be mapped into the pseudorapidity distribution. The higher the energy (and hence the Lorentz-boost) the more the rapidity plateau will be boosted into the forward cone. Fig. 3.22 demonstrates the acceptance for two typical incident energies, 10^{15} and 10^{16} eV, and for proton and iron interactions with oxygen. The fixed target pseudorapidity plateau is shown in a schematic way and the location of the center of the ALICE detector (90° in the center-of-mass system) is indicated. A CORAL acceptance of 0.1 and 1 mrad is indicated.

At the highest energies above 10^{16} eV, which correspond to the LHC energy there is a considerable overlap with the TPC of ALICE which covers ± 1 unit in pseudorapidity. At lower energies around 10^{15} eV the typical CORAL acceptance corresponds to very forward production which falls outside the ALICE acceptance.

We are in close contact with the ALICE collaboration to explore a common physics interest.

3.8   Milestones and Budget

3.8.1 Milestones

After approval, we will immediately begin to construct the air shower array. The construction of the platform and underground muon array will begin in spring 2002 when the civil engineering in the Intersection region 4 is terminated. We plan to begin taking data in the year 2003, and to continue for at least 3 years.

During summer 2001	Re-assembly of the 40 Kiel counters
	Construction of a calibration set-up for the surface counters
	Test and installation of the Kiel counters
	Test of the DAQ system and the GPS timing
	Test of all muon trigger counters
Autumn 2001	Coincidences between the I4 array and the L3C array at I2
	First physics results on extended air showers
2001/2	Construction of the gas system for the muon chambers
	Systematic tests of all muon chambers
	Construction of ~ 200 surface counters (India, Mexico) from existing material
	Continuous installation of the surface array
from spring 2002	Construction of the muon platform
	Installation of the gas system
	Installation of the muon chambers
	Read-out systems and DAQ
autumn 2002	First tests of trigger and read-out of both arrays
spring 2003	First test runs with the almost complete experiment
summer 2003	Begin taking data

3.8.2 Budget

As stated in the proposal, we have estimated about 915 kFS for the construction of the experiment. This investment will be spread over the first 3 years. In addition, 430 kFS are needed in the first three years for rental fees, consumables, maintenance and small upgrades. A contingency of 170 kFS is added to this budget. Following an investigation within the CORAL collaboration, we present in Tab. 3.6 the foreseen activities of each group and their contribution to the funding of the experiment. The estimates are based on initial discussions of the groups with their funding agencies and cannot be taken as full commitments at this stage of the proposal. It should be stressed that in-kind contributions, such as high-voltage supplies and controls of chambers and counters, are counted in these contributions, whereas salaries and travel expenses are not included.

	A	BG	Cern	CZ	FIN	D	IND J	MEX	PL	AM RU	USA
Infrastructure at I4											
Platform			X								
Muon chambers											
Install. UA1			X		X			X			X
” ” DELPHI				X					X		
” ” OPAL				X					X		
Gas system			X								
H.V. supplies + contr.		X									
DAQ + GPS	X		X		X					X	
Trigger logic	X		X		X					X	
Trigger counters underground										X	
Surface array											
HEGRA counters					X	X				X	
Indian counters							X				
Constr. new count.							X	X			
Test all counters		X	X		X	X	X	X			
H.V. for all counters		X									
Trigger, DAQ, GPS	X		X							X	
Maintenance + Consumption	X	X	X	X	X	X	X	X	X	X	X
Data Analysis											
Exp. simulation	X			X		X	X		X		
CR simulation			X	X					X		
Data analysis	X	X	X	X	X	X	X	X	X	X	X
Consumables (kFS)	5	5	5	5	5	5	5	5	5	5	5
Rental fee for electronics/year (kFS)			50								
Hardware contr./year for the first 3 years (kFS)	40	20	50	30	40	50	40	40	20	20	40

Table 3.6.

4   Additional Considerations

Since the presentation of the proposal we have started to recuperate drift chambers, electronics and counters from the DELPHI and OPAL experiments at LEP as well as from the HEGRA experiment at La Palma. The material is stored in several halls and four big containers. A list of the stored material is given below.

- Muon chambers available for the underground array (see Figs 4.1- 4.3):

Drift chambers	detection area per plane
UA1 chambers	~ 2200 m^2
DELPHI chambers	~ 1000 m^2
OPAL chambers	~ 1000 m^2
Total	~ 4200 m^2

- Trigger counters for the muon array from DELPHI (Fig. 4.4):

Eight double layers of counters are placed in one support box. 14 such boxes were constructed and equipped with counters for CORAL. The total area of ~ 70 m^2 with 112 double layers of counters will be distributed over the muon chamber array and will provide an excellent multi-muon trigger.

- Scintillation counters for the surface array:

from the Hegra experiment	
40 Kiel counters (1 m^2 each) completely equipped	40 x 1.0 m^2
Material (photomultipliers, scintillation plates,...)	150 x 0.5 m^2

from India	
50 flat counters with fiber read-out presently used in L3C	50 x 0.5 m^2

References

[1] *"CORAL: A Cosmic Ray Experiment in and above the LHC tunnel"*, CERN/SPSC 2001-003,SPSC/P321, 08.01.2001.

[2] FELIX Collaboration, "FELIX, A Full Acceptance Detector at the LHC", CERN/LHCC 97-45, LHCC/I10, August 1997.

[3] T. C. Brooks, *et al.* [MiniMax collaboration], Phys. Rev. **D61** (2000) 032003 [hep-ex/9906026], and references therein.

[4] T. C. Brooks, *et al.* [MiniMax collaboration], Phys. Rev. **D55** (1997) 5667 [hep-ph/9609375].

[5] C. M. G. Lattes, *et al.*, Physics Reports **65** (1980) 151; S. Hasegawa, ICRR Report 151-87-5 (1987).

[6] J. J. Lord and J. Iwai, Paper 515, presented at the International Conference on High Energy Physics, Dallas (1992); H. Wilczynski *et al.*, Proceedings of teh XXIV International Cosmic Ray Conference, HE Sessions, Rome (1995), v. 1, p. 1.

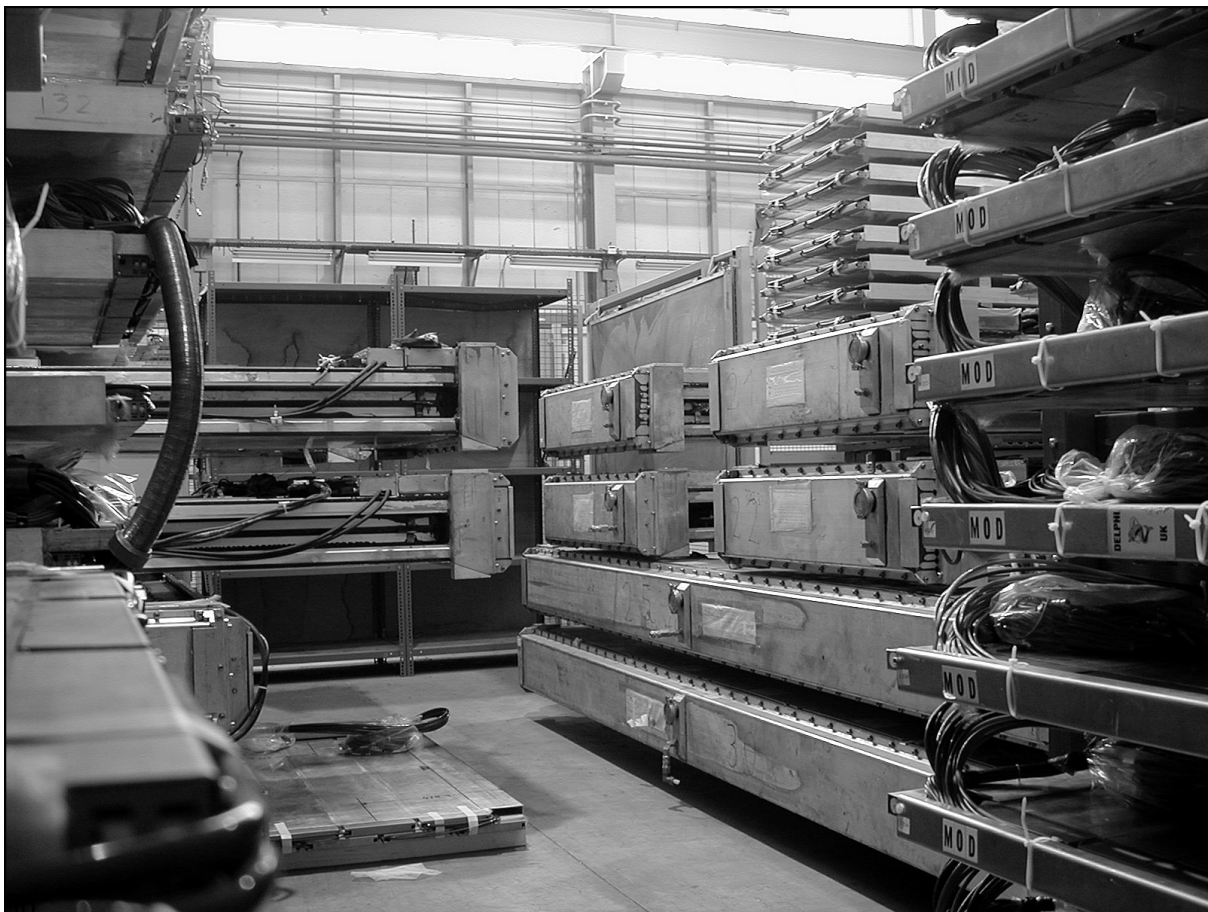*Figure 4.1. UA1 and DELPHI muon chambers in hall 167.*

Figure 4.2. UA1 and DELPHI muon chambers: a closer view.

Figure 4.3. OPAL chambers in hall 157.

Figure 4.4. Some of the muon trigger counters.